View metadata, citation and similar papers at core.ac.uk

brought to you by CORE

provided by NASA Technical Reports Server

NASA-CR-204107

A Final Report to the National Aeronautics and Space Administration

Fabrication and Characterization of a Long Wavelength InP HBT-Based Optical Receiver

NASA Grant NAG3-1757

K. P. Roenker
Department of Electrical and Computer Engineering and Computer Science
University of Cincinnati
Cincinnati, Ohio 45221-0030

April 5, 1997

Project Period: June 1, 1996 - December 31, 1996

Kenneth P. Roenker
Professor of Electrical and
Computer Engineering

1. Introduction

The use of optical signals for transmission and distribution of high frequency signals has received much attention recently for such applications as phased array antennas, optical telecommunications, computer interconnections (LAN) and cable television distribution [1-5]. These developments have resulted in part due to the huge bandwidth capability of the optical fiber (> 500 GHz) and their low attenuation losses (< 0.5 dB/km). Current applications are employing frequencies in the few GHz regime, which are limited primarily by the speed at which the transmit and receive electronics can operate at each end of the fiber where the optical signals are generated and injected, and detected and amplified, respectively[4,5]. Ongoing developments in the research laboratory are expected to continue to open new opportunities for commercial applications and expand existing ones including the evolution of the operational speed of such systems to much higher frequencies, even above 30 GHz. This is possible because the transistor and optoelectronic device performance are continuing to evolve in the research laboratory where some prototype transistors have, for example, been demonstrated with gain well above 100 GHz [6,7]. In addition, the simultaneous fabrication (monolithic integration) of optical and electronic devices on the same semiconductor substrate to produce optoelectronic integrated circuits (OEIC's) is expected to reduce fabrication costs, improve system reliability, and reduce dramatically the parasitics which limit high frequency performance.

In recent years there have been a number of published reports of InP-based heterojunction bipolar transistor (HBT) which have demonstrated the device's outstanding potential for use in high speed integrated circuits (IC's) and optoelectronic integrated circuits (OEIC's)[6-8]. The InP/InAlAs/InGaAs material system is particularly attractive because it is also suitability for fabricating high performance optical devices, such as high speed photodetectors which can operate in the long wavelength regime (1300-1550 nm). Hence, the possibility exists that both the optical and electronic devices can be fabricated on the same semiconductor substrate using these InP-based materials and that OEIC's can be produced with sufficiently high frequency performance.

The thrust of this work has been to develop as a high speed photodetector the InP-based phototransistor (HPT) for use in optical receivers for microwave signal distribution for satellite phased array antennas. Currently, p-i-n photodetectors are used because of their compatibility with the heterojunction bipolar transistor (HBT), but their performance limits the bandwidth of these optical receivers [8]. The HPT photodetector was investigated here as an alternative photodetector for monolithic integration with heterojunction bipolar transistor

amplifiers in long wavelength (1.3 μm), gigahertz (GHz) frequency optical receivers. These phototransistors are attractive because they provide optical gain, which improves receiver sensitivity and signal-to-noise [9,10]. But, to date, they have not received as much attention and so are relatively undeveloped. For example, their high frequency operation has not been adequately demonstrated, though they have intrinsically the same high frequency capabilities of the closely related HBT [9,10]. In addition, the use of the dc bias to the base, i.e. the three terminal configuration for device operation, has not been extensively examined, either theoretically or experimentally, though there have been some reports of encouraging results [11-13].

To date, the primary obstacle to the development of optical receivers that can operate at and above 10 GHz has been that the photodetector limits the high frequency performance [8]. One objective of this project has been to design, fabricate and test an alternative photodetector, i.e. the heterojunction bipolar phototransistor (HPT) [9,10], in the InP-based material system that can achieve the necessary high frequency performance [11-13], and yet be suitable for monolithic integration with the transistor amplifier in the optical receiver. Our group has been working for some time to develop a capability for the simulation and design of the InP-based phototransistors (discussed below) and some initial results have been reported [14-17]. This work is an outgrowth of previous work on the modeling of the related InP-based HBT [18], which was also needed for the design and simulation of these optical receivers. Described briefly below is the phototransistor's structure and operation. Presented are simulation results of its expected performance based on a device model for the three terminal configuration. In particular, an improved theoretical description of the device's operation has been developed by us that incorporates the physics of the device's emitter-base heterojunction as well as the effects of optical absorption in the base, base-collector space charge region and collector [14,15]. Further development of this model has also been pursued to more accurately predict the device's optical gain and high frequency performance. In particular, development of a more complete Gummel-Poon model has been achieved that includes all of the base recombination currents and a description of the effects of high optical injection [16,17]. This development of a device simulation capability has been supported by a parallel effort in the experimental fabrication and characterization of these devices and recievers. Described in the following sections are the results achieved to date in each of these areas.

II. Experimental Work

Shown in Figure 1 below is the phototransistor's energy band diagram, top-view layout, cross-sectional structure, and its multi-layer epitaxial structure. The device's mesa structure seen in Figure 1(c) was formed using wet chemical etching and selective removal of semiconductor layers, and metal and dielectric depositions and etchings, all incorporated in a ten mask fabrication process. To contain the substrate and fabrication costs, constrain the complexity in the fabrication and achieve good fabrication yield, the same fabrication process steps and epitaxial layer structure are employed, as much as is possible, for both the fabrication of the phototransistor and the HBT transistor used in the photoreceiver's preamplifier [6,8].

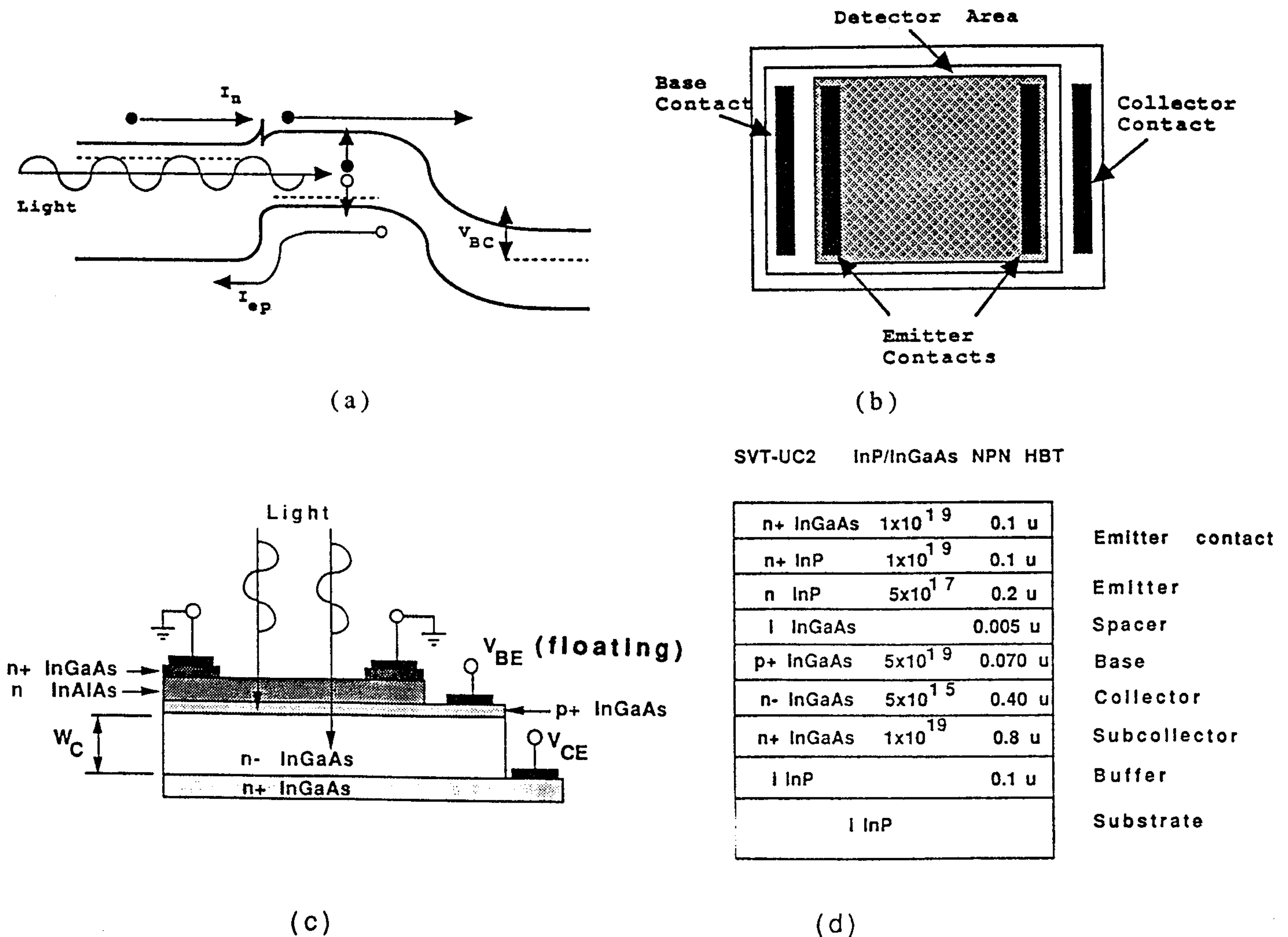

Figure 1 Energy band structure(a), top view(b), and cross-sectional view(c) of InP-based heterojunction phototransistor(HPT) and device's epitaxial layer structure (d).

The above described InP-based heterojunction phototransistors (HPT's) were fabricated on campus using available facilities in the department's microelectronics fabrication facility. The starting substrate contained the epitaxial structure shown in Figure 1 (d), which has been recently grown by SVT Associates. Recently, a second wafer was obtained from Hughes Research Laboratories with an InAlAs emitter, but otherwise nearly the same epitaxial structure. Seen in Figure 2 (a) below is an SEM picture of the finished HPT showing the device's mesa structure and its large, square detector area with two emitter contacts near the top left and bottom right. This allows the device to be illuminated from above between the emitter contacts. Seen in Figure 2 (b) is a second SEM of an HPT with the smaller device at the lower right a conventional HBT that is subsequently incorporated in the preamplifier of the optical receiver.

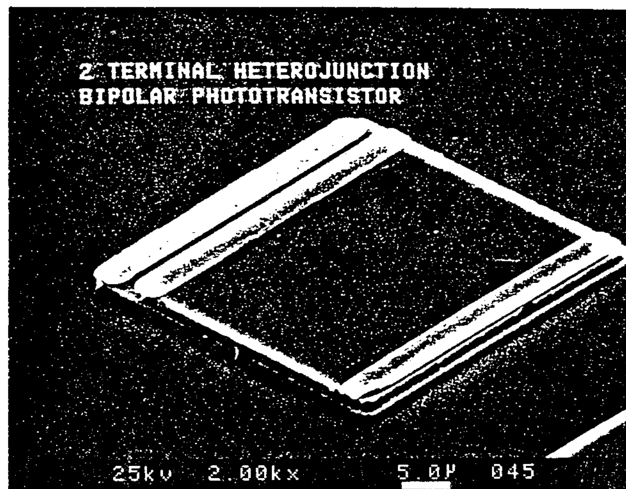

(a)

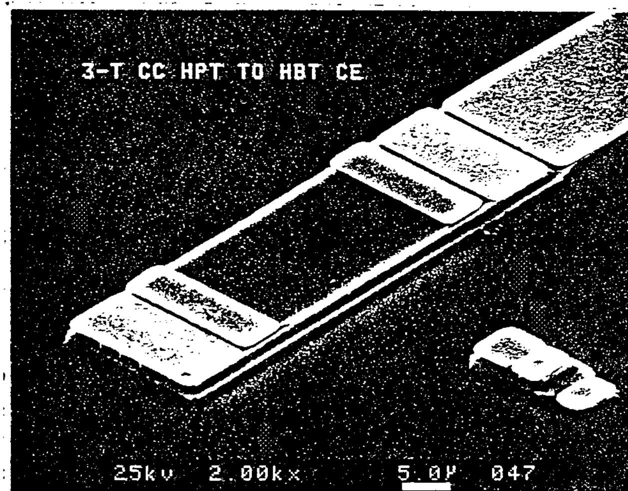

(b)

Figure 2 SEM of finished HPT (a) and SEM of HPT with smaller adjacent HBT (b) subequently connected in an optical receiver.

During characterization, when the device was operated in the two terminal configuration, its equivalent circuit is that seen in Figure 3 (a) [9] and the optical response characteristics of the HPT phototransistor with a 10 μm x 10 μm emitter, where each curve corresponds to a different light intensity (0 dB = 1 mW), are seen in Figure 3 (b). As can be seen from the equivalent circuit, the light absorption generates a photocurrent that constitutes an input current to the device's base so that the transistor's current gain produces an optical gain for the phototransistor. For this particular substrate, the optical gain G is only about 1.5 and the responsivity R is 1.7 mA/mW. Much higher optical gains and responsivities are expected for the phototransistor. The low responsivity and optical gain in this case are due to the relatively poor current gain provided by the device's transistor action, which is due to the poor quality of the epitaxial growth and structure.

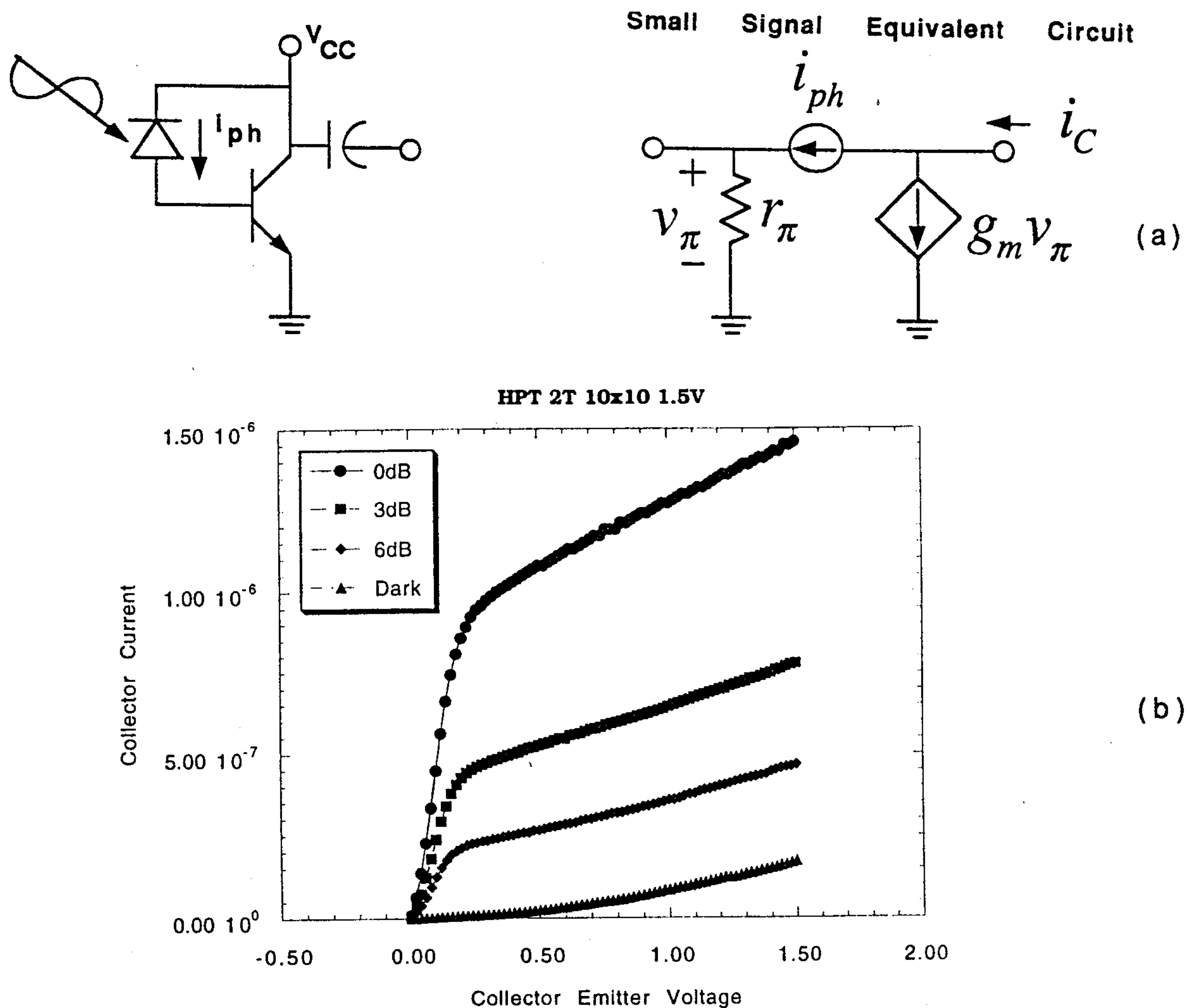

Figure 3 Equivalent circuit (a) and optical response characteristics (b) for an HPT with 10 μm x 10 μm emitter operated in two terminal configuration (base floating).

To improve the transistor's current gain and its optical gain, the HPT can be operated in the three terminal configuration, i.e. with a DC bias applied to the base as shown in Figure 4 (a). The corresponding equivalent circuit is shown in Figure 4 (b).

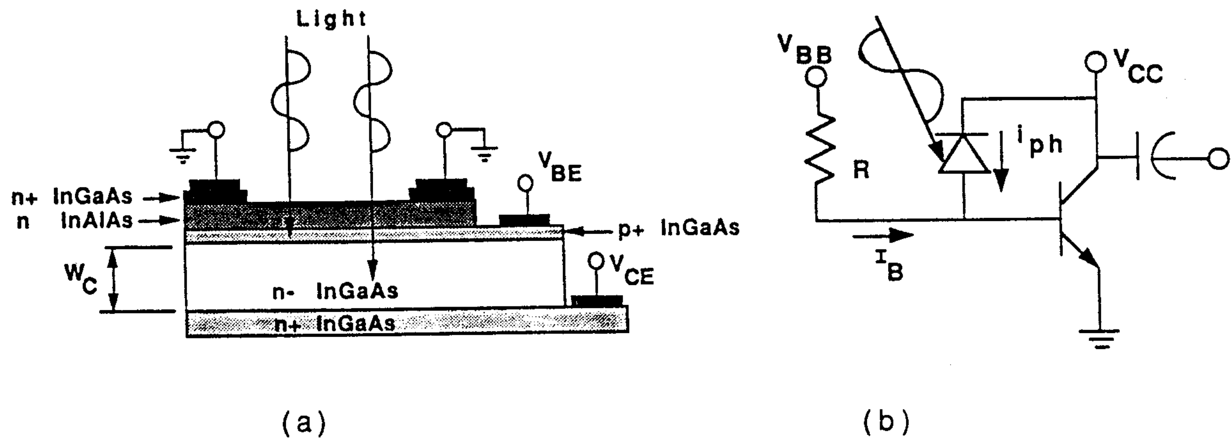

(a) (b)

Figure 4 HPT operation in the three terminal configuration (a) and equivalent circuit (b).

Shown in Figure 5 are the experimental results obtained for the same size HPT operated with a DC bias on the base. Figure 5 (a) shows the transistor's current-voltage characteristics in the dark, while (b) shows them for a 1 mW light intensity. As the dark I-V characteristics show, the transistor exhibits only a modest gain of about 5 for a V_{CE} of 1 V and a base current of 40 µA. This is due to the poor quality of the epitaxial structure used to build the devices, as discussed above for the two terminal operation of the HPT. As a result of this low current gain, the I-V characteristics in the case of optical illumination at 1 mW (Figure 5 (b)) show nearly the identical I-V characteristics. This is because the total photocurrent generated (as seen in Figure 3) is only about 1 µA for the 1 mW illumination. This is due in part to the large spot size, approximately 200 µm radius. Because of this small photocurrent, which becomes the base current for the HPT, and because the current gain is only 5, the HPT generates a corresponding collector photocurrent of only 5 µA. Since the total collector current for a base current of 40 µA (as seen in Figure 5 (b)) is about 120 µA (corresponding to a current gain of 3), the optical contribution is small. However, for normal HBTs, a current of gain of 100 or more is typical so that the same 1 µA base photocurrent for the 1 mW illumination would be expected to generate more than 100 µA for the collector current, which would be easily seen and provide the high responsivity (> 10 mA/mW) and optical gain anticipated for these devices. Further optical measurements are in progress on devices recently fabricated on the Hughes wafer for which the current gain is much larger, i.e. approximately 50-80, so much better optical gains are expected.

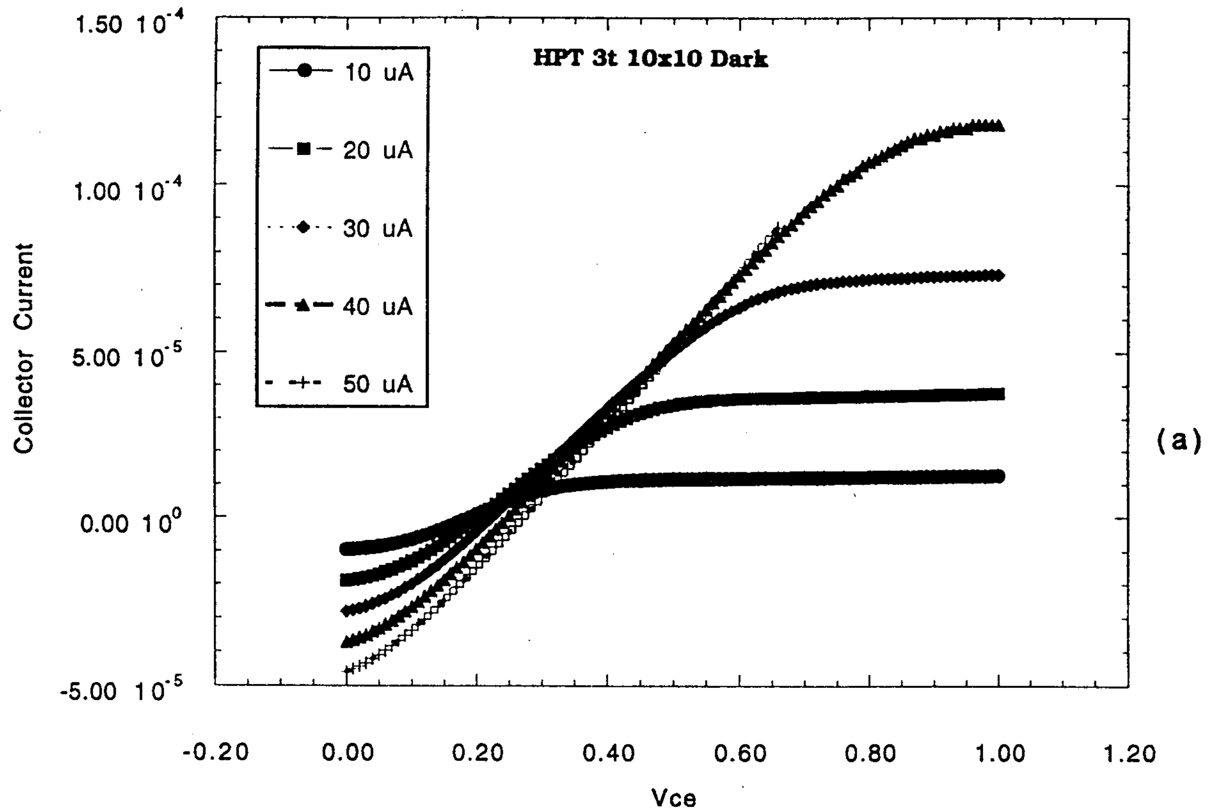

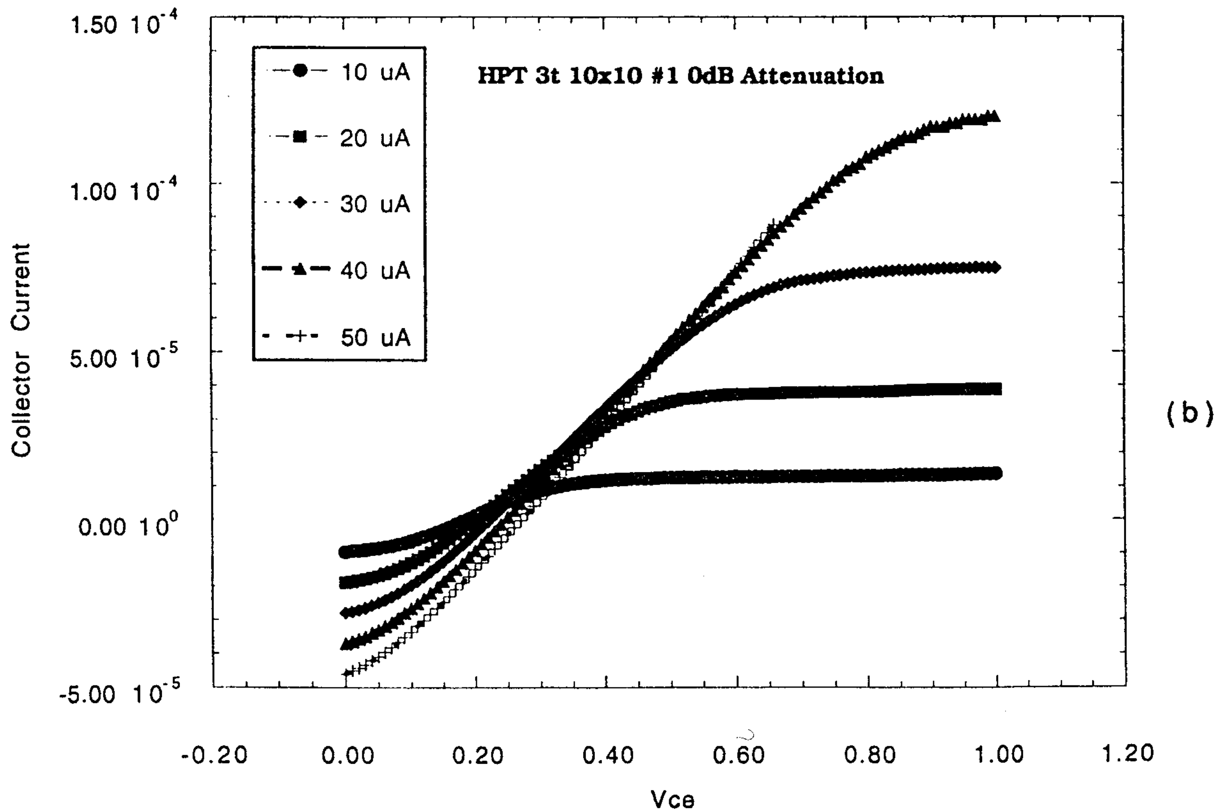

Figure 5 Current-voltage characteristics for the HPT operated in the three terminal configuration for no light (a) and for a 1 mW optical illumination (b).

Recently we have obtained an HBT wafer from Hughes Research Laboratories with a similar epitaxial structure but with a superior epitaxial quality. Shown in Figure 6 (a) below is the wafer's epitaxial structure while seen in Figure 6 (b) is a double crystal x-ray spectrum for the wafer.

Layer	Doping	Thickness	
n+ InGaAs	$1x10^{19}$	0.1 u	Emitter contact
n+ InAlAs	$1x10^{19}$	0.07 u	
n InAlAs	$8x10^{17}$	0.12 u	Emitter
n-p InAlAs-InGaAs		0.03 u	Graded layer
p+ InGaAs	$2x10^{18}$	0.010 u	Spacer
p+ InGaAs	$4x10^{19}$	0.060 u	Base
n- InGaAs	$5x10^{15}$	0.70 u	Collector
n+ InGaAs	$1x10^{19}$	0.7 u	Subcollector
i InGaAs		0.01 u	Buffer
i InP			Substrate

(a)

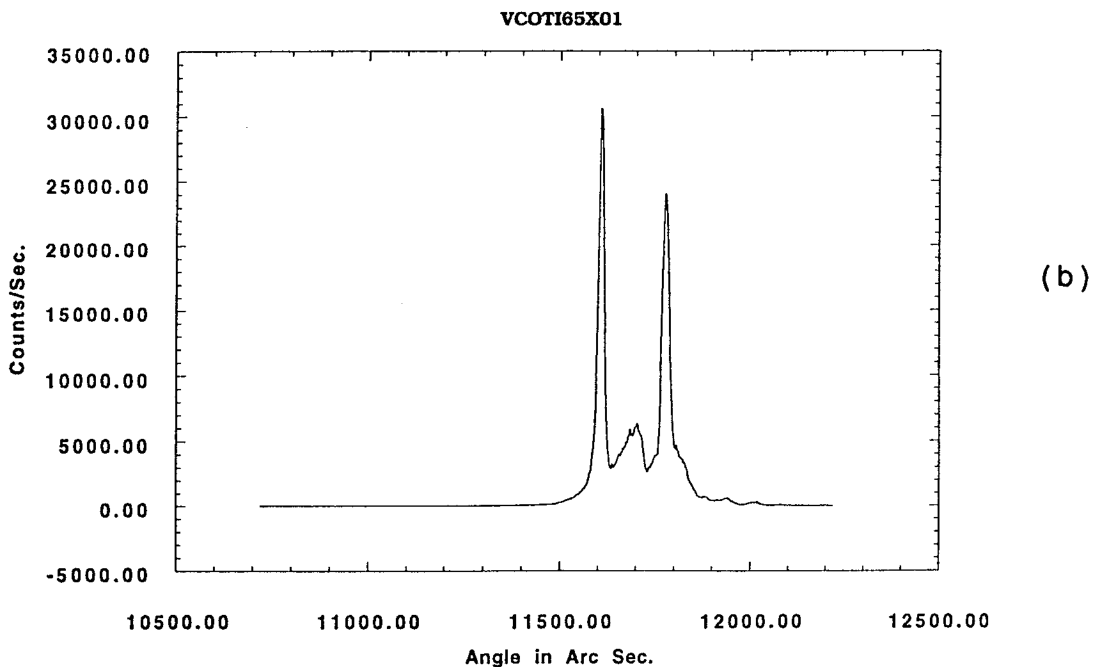

(b)

Figure 6 Epitaxial multi-layer structure (a) and double crystal x-ray spectrum (b) for InAlAs/InGaAs HBT wafer grown by Hughes Research Laboratories.

Seen in Figure 7 (a) below are the DC output characteristics of the device and in Figure 7 (b) the Gummel plot of the base and collector currents versus base-emitter bias. As can be seen, the device exhibits a sizable current gain of 20 to 50 so that the HPT can be expected to exhibit much better optical gain than that reported above. Hughes has reported similar results for this epitaxial structure [19,20].

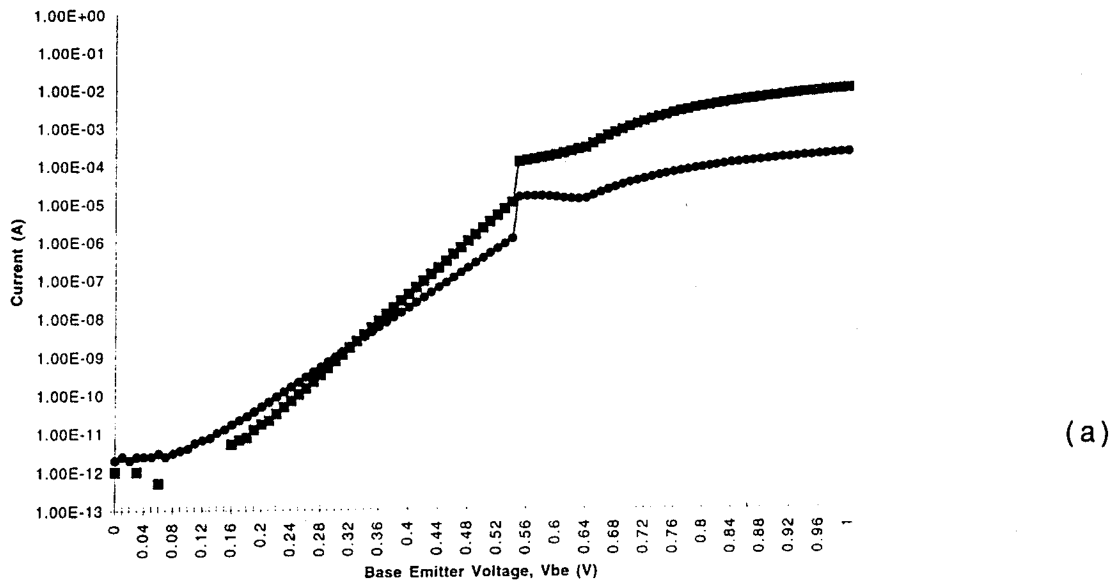

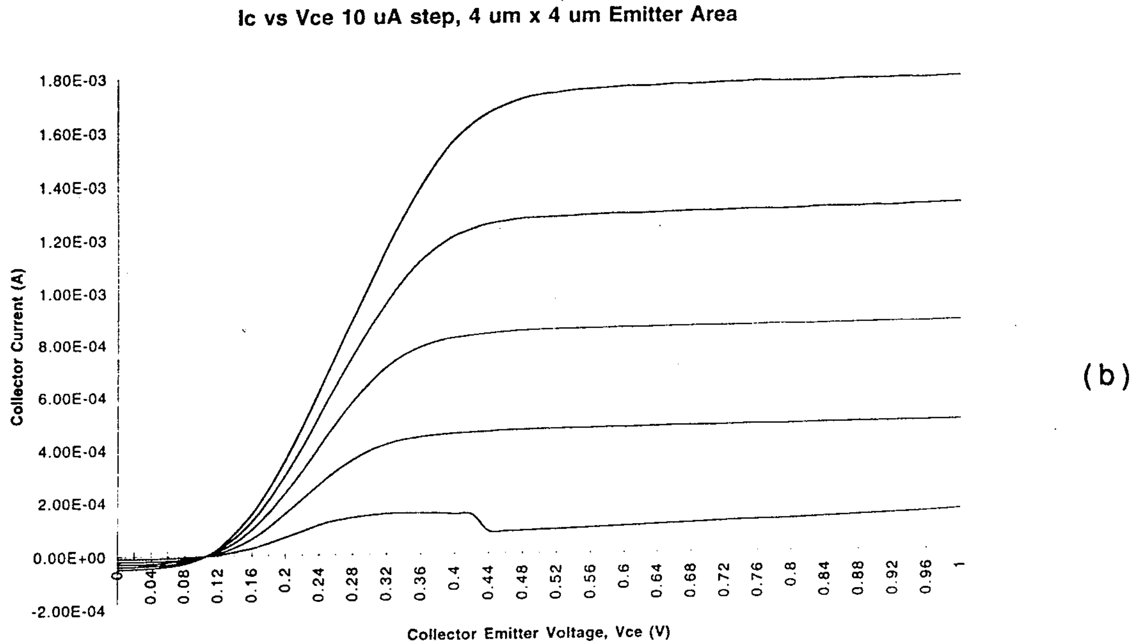

Figure 7 Experimental device output characteristics (a) and Gummel plot (b) for a transistor with a 4 μm x 4 μm emitter fabricated in Hughes wafer.

Preliminary microwave measurements have also been performed on the transistors and phototransistors fabricated using the Hughes wafer. Shown in Figure 8 are the microwave results for a 10 µm x 10 µm emitter HPT showing a cutoff frequency of 7.1 GHz biased at a collector current of 25 mA. As described in our theoretical analysis discussed in the following section [14-16], the device's performance is a function of the DC base biasing of the transistor, so further experimental work is planned to examine the effects of the biasing.

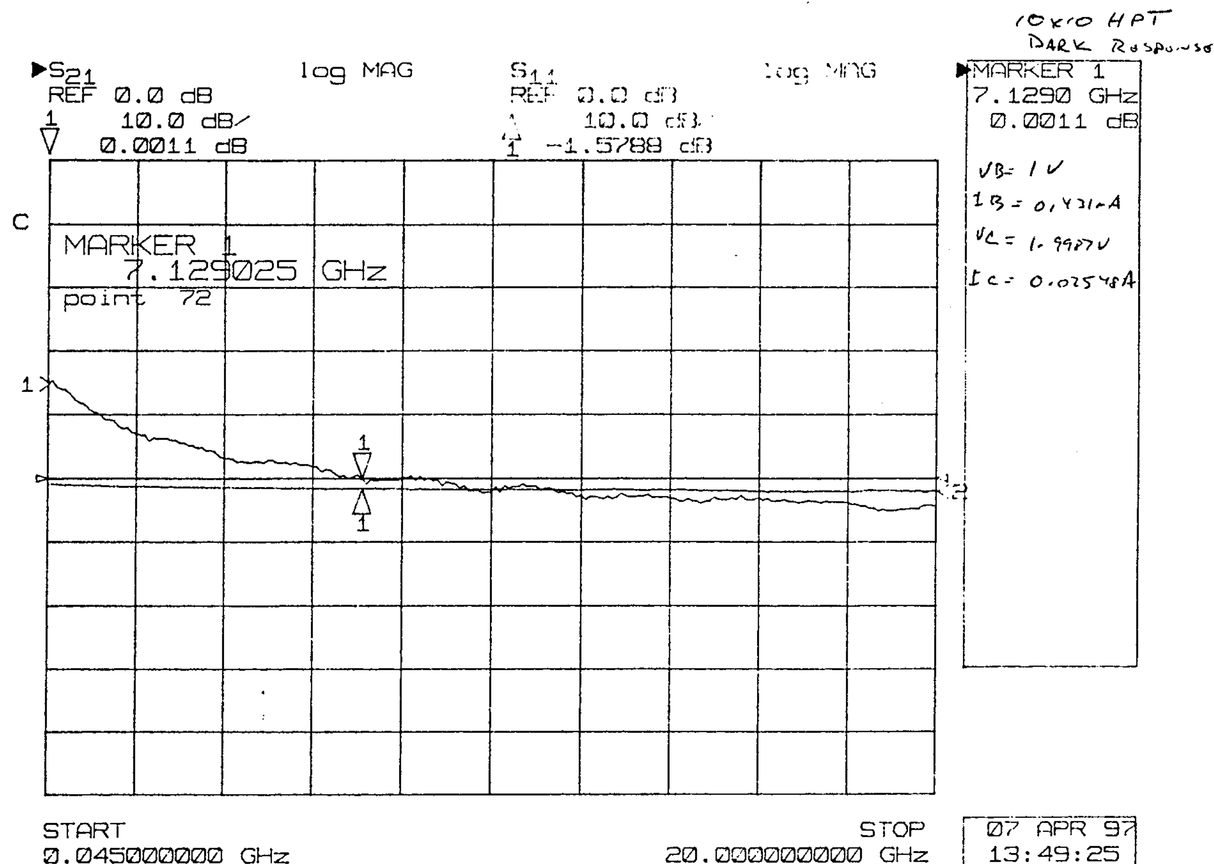

Figure 8 Microwave measurements of a 10 µm x 10 µm emitter HPT biased at a collector current of 25 mA showing a cutoff frequency of 7.1 GHz.

Shown for comparison in Figure 9 are the microwave results for a larger 100 µm x 100 µm emitter HBT showing a cutoff frequency of nearly 30 GHz. For the same epitaxial structure and a very similar fabrication process, Hughes have measured a cutoff frequency for the small area transistor above 100 GHz as shown in Figure 10 [19,20] so that considerably higher frequency operation of our phototransistors is expected to be feasible. We are currently reprocessing one of our samples to overcome a high series resistance problem associated with our fabrication process which we believe is limiting the high frequency performance of these devices.

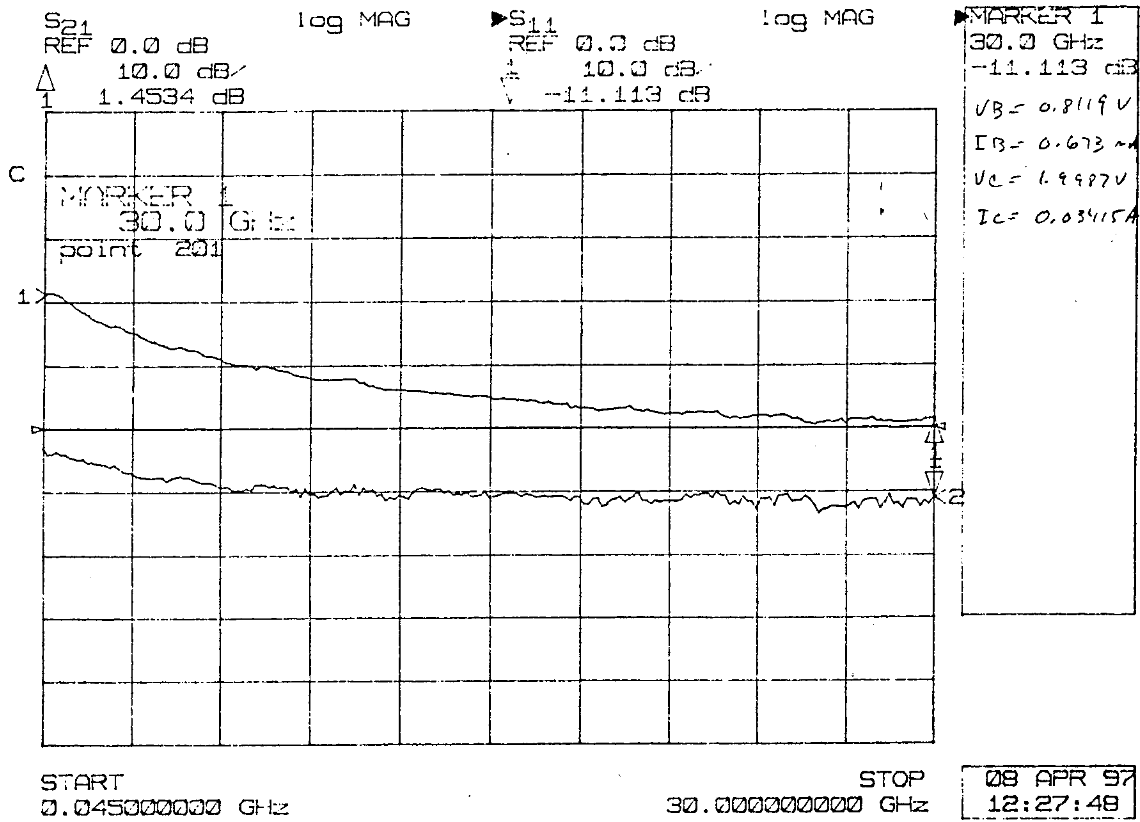

Figure 9 Microwave results for a large 100 μm x 100 μm emitter HBT showing a cutoff frequency of 30 GHz.

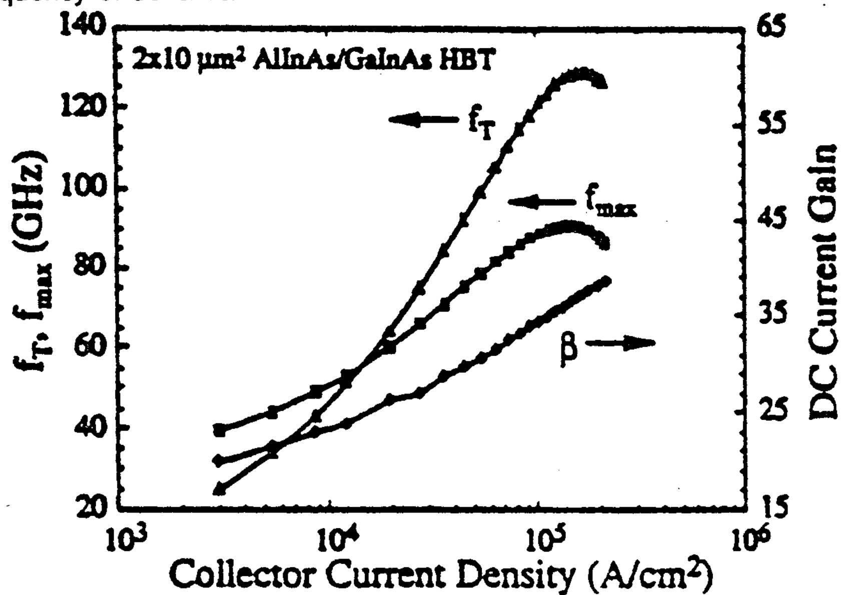

Figure 10 Measured current gain and cutoff frequency results reported by Hughes for the same epitaxial structure and a similar fabrication process [19,20].

III. HPT Simulation Results

The rationale for employing the HPT instead of the conventional P-I-N photodiode is based on a performance comparison performed recently and reported [16]. The results are summarized in the following figures and discussion. Seen in Figure 11 is a plot of the cutoff frequency (maximum frequency of operation) versus the I-region thickness for the P-I-N or collector thickness for the HPT. For the P-I-N or HPT integrated with an HBT-based amplifier in a receiver, these are necessarily the same layer and thickness. As the figure shows, for the P-I-N, a thicker collector is desired to enhance the cutoff frequency since the device's capacitance limits its speed and that capacitance decreases as the I-region thickness increases. For the HPT, the cutoff frequency is considerably larger since the device's speed is not primarily controlled by the collector thickness, but rather by the base thickness. Also shown in Figure 11 is the dramatically better responsivity expected for the HPT due to the transistor's current gain relative to the P-I-N.

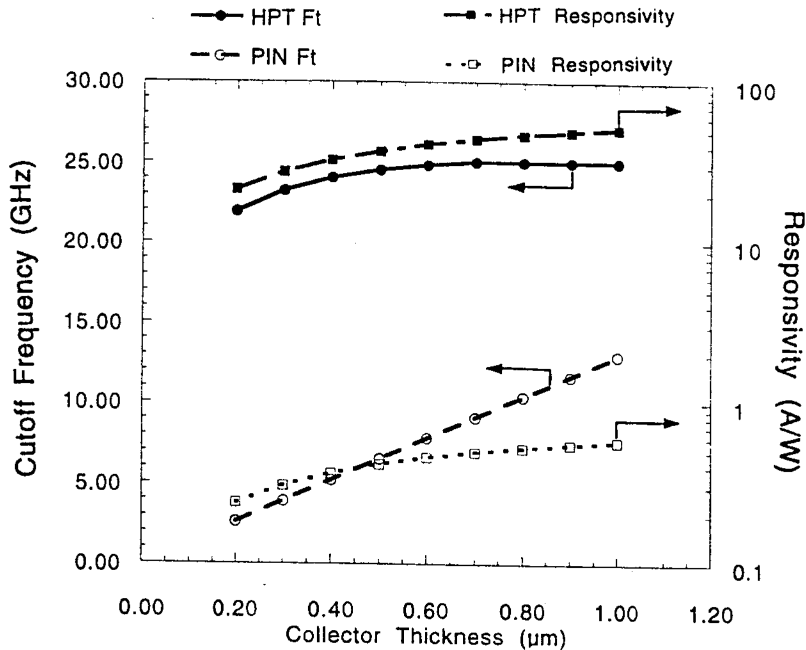

Figure 11 Comparison of the cutoff frequency and responsivity for the P-I-N and HPT as a function of the collector (I-region) thickness.

Seen in Figure 12 are the effects of the collector doping on the performance for the two devices. While a light doping is desirable for the P-I-N so that its I-region can be depleted with a reasonable applied bias, the HBT (and HPT) desires a larger collector doping to get higher

speed operation. As a result, there is a tradeoff in the selection of the collector layer doping for the P-I-N photodetector design relative to the HBT's (and HPT's) design. Since the HPT operates in very nearly the same manner as the HBT, there is not the same tradeoff in the HPT-HBT receiver design. Optimization of the collector doping for the HBT will also optimize it for the HPT.

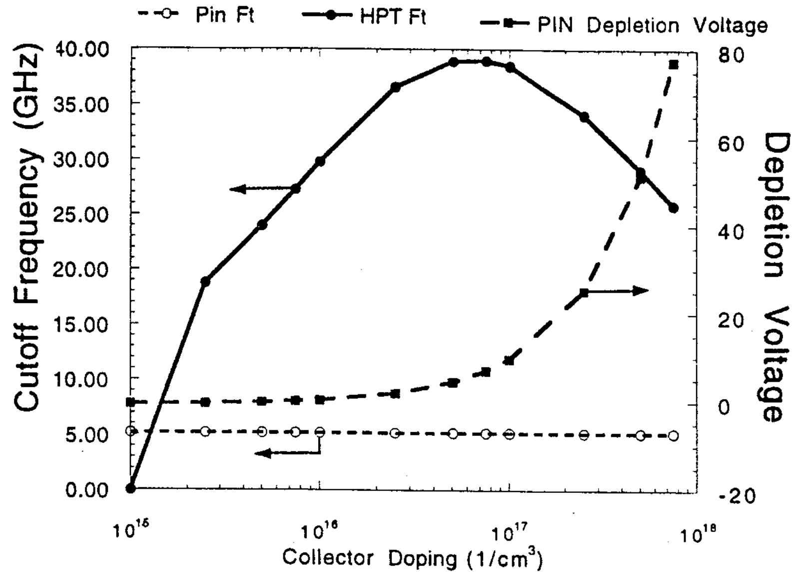

Figure 12 Comparison of the cutoff frequency and responsivity for the P-I-N and HPT as a function of the collector (I-region) thickness doping.

A related issue for comparison of the P-I-N and HPT are the effects of the detector size on the photodetector performance. Seen in Figure 13 are the cutoff frequency and responsivity of the two devices plotted versus the detector area. For the P-I-N, the device's speed goes down dramatically as the device size increases since the device capacitance scales with the area. Even for a reasonably small detector, e.g. 10 μm x 10 μm, the P-I-N's cutoff frequency is down to 5 GHz. The issue of device size is important for coupling of the optical signal into the device from an optical fiber. Due to spreading of the optical beam as it emerges from the end of the fiber, the detector size and spacing of the detector relative to the end of the fiber are important. If the beam is small, either due to focusing or a close spacing to the end of the fiber, then precise alignment of the detector is needed, which increases the difficulty in alignment and can increase production costs. As a result, a somewhat larger detector is attractive to easy alignment requirements and to capture more of the optical beam due to its spreading.

By comparison, for the HPT the cutoff frequency remains high and nearly constant as seen in Figure 13. But this is the case only if the device is biased at the same collector current density. The consequence of this is that the collector current then scales up in direct relation to

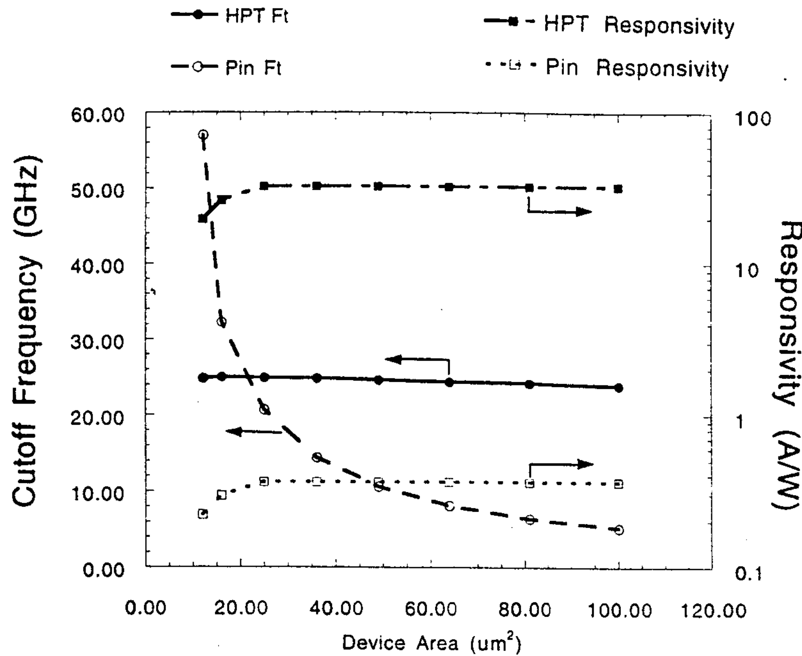

Figure 13 Cutoff frequency and responsivity versus detector area for P-I-N and HPT.

the transistor size so that the associated shot noise similarly rises. This will, in turn, affect the signal-to-noise ratio exhibited by the phototransistor. But for the HPT, if the optical beam size is larger than the phototransistor, as is usually the case, then the increase in the device size will also result in a larger signal so that the net effect on the signal-to-noise is not clear. It will depend on the relative size of the various noise components as to the net effect of the increase in device area on the phototransistor's signal-to-noise ratio. However, due to the HPT's current gain, it may be possible to keep the device small and obtain a sufficiently large signal. By contrast, the P-I-N does not provide an optical gain, so collection of most of the optical beam is essential to get an adequate signal. The HPT's small size would then allow operation at a lower collector current and associated noise level. This small size would also assist in obtaining the desired high frequency performance from the device. In summary, the HPT appears to offer an attractive alternative to the P-I-N photodiode for HBT-based optical receivers whose development has been pursued in this work.

In addition to the experimental development of the phototransistor, a second major objective of the proposed work is to continue our development of an improved theoretical model for the HPT. In particular, what is needed is a more comprehensive model for the HPT, particularly for describing its operation in the three terminal configuration as shown in Figure 4 (a) where a DC bias current is supplied to the device. Because of the HPT's similarity in

structure and operation to the HBT, the device's small signal current gain and optical gain are a function of the DC base and collector currents, increasing to a maximum at some high, finite value before high injection effects produce a falloff. While the HPT has been explored and theoretically described when operated in the two terminal (floating base) configuration[9,10], this is far from the optimal biasing since the DC collector current is extremely small (almost, but not zero). Hence, improved device performance can be expected if a simple DC bias is applied to the base and set appropriately to maximize the small signal current gain. Experimentally, there have been a number of recent reports of improved HPT performance when the base is provided with a DC bias [9,10,12,13,21].

Recently, we have reported the development of a thermionic-field-diffusion model for use in the analysis and design of abrupt, single heterojunction bipolar phototransistors for use in HBT-based optical receivers [14]. In particular, included in this approach are the effects of a dc base bias on the optical gain and device performance. Taking into account the optical generation, the excess electron concentration at the emitter end of the quasi-neutral base is initially determined using a matching of the thermionic field emission across the emitter-base heterojunction with the diffusion current at the emitter end of the base. This model is also an improvement over two terminal descriptions of the device's operation [9,10] in that it includes a more accurate description of the electron injection process from the emitter into the base following Grinberg et al. [22]. In addition, at the collector end of the base region, a finite electron concentration is used based on the collector current density following Das [23]. These two results are then used to more accurately determine the electron profile in the quasi-neutral base region and the diffusion components to the emitter and collector currents. To determine the device's optical gain, the photocurrent and the phototransistor's small signal current gain are calculated and combined. Described briefly below are some of the results obtained thus far with this improved model.

The above mentioned thermionic-field-diffusion model provides a means for estimating the performance for the three terminal operation of the HPT and for examining design issues and tradeoffs, particularly in the selection of the epitaxial layer parameters. In this section we calculate the photocurrent density and optical gain at 1.3 μm for an InP/InGaAs HPT using the materials parameters summarized in Table I [18], which are similar to those of Chandrasekhar et al. [21] and Scott and Fetterman [10]. Seen in Figure 14 is a comparison of the calculated and measured optical gain G as a function of the collector current for the device structure of Chandrasekhar et al. [21] (12 x 12 μm^2 emitter) operated in the three terminal configuration, for an optical power of 1 μW and biasing of V_{CC} = 2 V. It is important to note here that the above

Table I
Material Parameters for NPN InP/InGaAs Heterojunction Phototransistor

Emitter	Base	Collector
InP n-type	InGaAs p-type	InGaAs n-type
$N_E = 5 \times 10^{16}/cm^3$	$N_B = 7 \times 10^{17}/cm^3$	$N_C = 5 \times 10^{15}/cm^3$
$W_E = 0.2\ \mu m$	$W_B = 0.20\ \mu m$	$W_C = 1.0\ \mu m$
$L_{pe} = 10.3\ \mu m$	$L_{nb} = 2.25\ \mu m$	$L_{pc} = 2.9\ \mu m$
$D_{pe} = 3.7\ cm^2/sec$	$D_{nb} = 146\ cm^2/sec$	$D_{pc} = 8.55\ cm^2/sec$
$\mu_{pe} = 143\ cm^2/V\ sec$	$\mu_{nb} = 5642\ cm^2/V\ sec$	$\mu_{pe} = 331\ cm^2/V\ sec$
$\alpha_e = 0.00/\mu m$	$\alpha_b = 1.50/\mu m$	$\alpha_c = 1.50/\mu m$
$m_{ne}^* = 0.075\ m_o$	$m_{pb}^* = 0.47\ m_o$	
$\eta_e = 1.0$	$\eta_b = 1.0$	$\eta_c = 1.0$
$S_e = 10^4\ cm/sec$	$\tau_n = 0.35\ nsec$	$S_c = 0\ cm/sec$
	$v_{sat} = 8.0 \times 10^6\ cm/sec$	

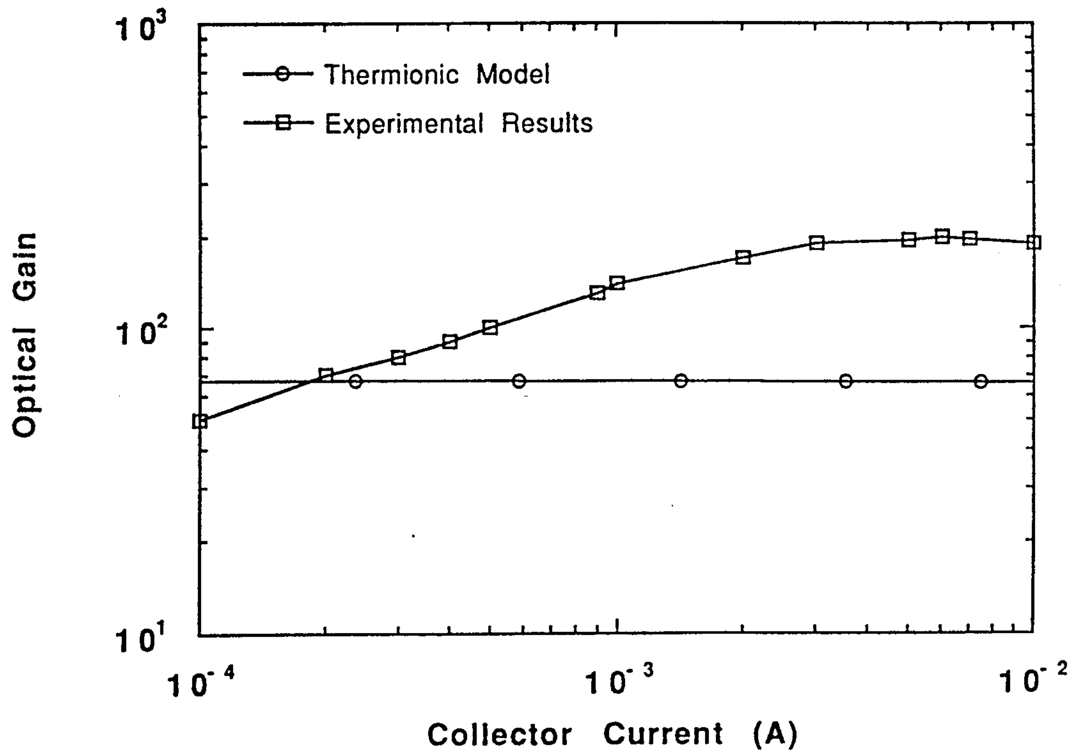

Figure 14 Calculated and measured optical gain versus collector current for the device structure of Chandrasekhar et al. [21] for an optical power of 1 μW and biasing of $V_{CC} = 2$ V.

described thermionic-field-diffusion model was derived assuming frontside illumination, i.e. light penetration through the emitter, but where the n+InGaAs emitter contact layer was assumed to be removed except under the emitter metal contacts. By contrast, for the device results reported by Chandrasekhar et al. [21], backside illumination, i.e. through the subcollector (InP), was employed. As a result, exact agreement between the experimental and simulation results cannot be expected. However, since there is little other data currently available for the three terminal configuration for the HPT for comparison, the data of Chandrasekhar et al. [21] has been used here.

As seen in Figure 14, the HPT's calculated optical gain is nearly constant and independent of the collector current. This latter effect is because we have neglected in this model to include all of the recombination currents in the determination of the base current and the current gain, which is discussed further below. In addition, we note from Figure 14 that the calculated optical gain underestimates the experimental results at the higher collector currents by a factor of about three. This can be explained, in part, from the fact that the collector component is underestimated in our model because of our assumption of frontside illumination, whereas the experimental results were derived using backside illumination. As seen in Figure 15, absorption in the base-collector space charge region produces the largest contribution to the photocurrent for the case of frontside illumination, but the collector component contributes significantly as well. For backside illumination, the collector component would be enhanced while the base-collector space charge region absorption would be reduced. As a first order approximation taking into account only the optical absorption in the intervening layers, the photocurrent components for the backside illumination case can be estimated from the results in Figure 15 for frontside illumination. For the device of Chandrasekhar et al. [21], we estimate that the collector component would be increased by a factor of nearly four while the base-collector space charge region absorption would be reduced by a factor of about three, due to increased absorption in the thicker collector. The net result is that the total photocurrent, and so the optical gain, would be increased by approximately 20%. While this would bring the simulation and experimental results closer, there would remain a significant degree of underestimation in the calculated results which remains unexplained. Of course, this simple calculation of the photocurrent components does not take into account the details of the profile of the excess, optically generated carriers which may also impact the results to some extent. More likely, the underestimation is due to the fact that this model produces a conservative estimate of the current gain, which is calculated to be approximately 100 for the device of Chandrasekhar et al. [21] as shown in Figure 16. By comparison, Chandrasekhar et al. [21] report current gains from 90 to 800 depending upon the collector current density.

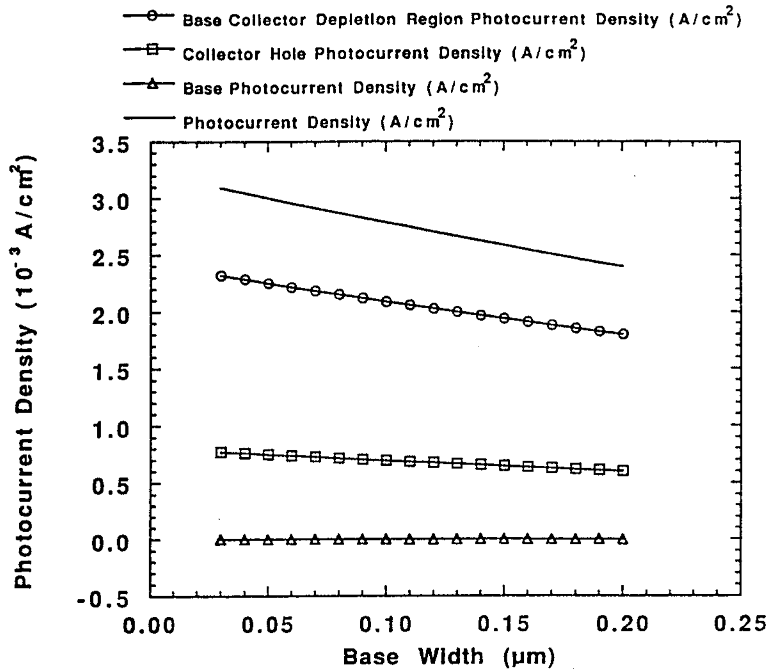

Figure 15 Total photocurrent density and quasi-neutral base, base-collector space charge region and collector region components versus base width W_B for the device structure of Chandrasekhar et al. [21] for a base doping of 7 x $10^{17}/cm^3$ for a constant optical power of 1 μW.

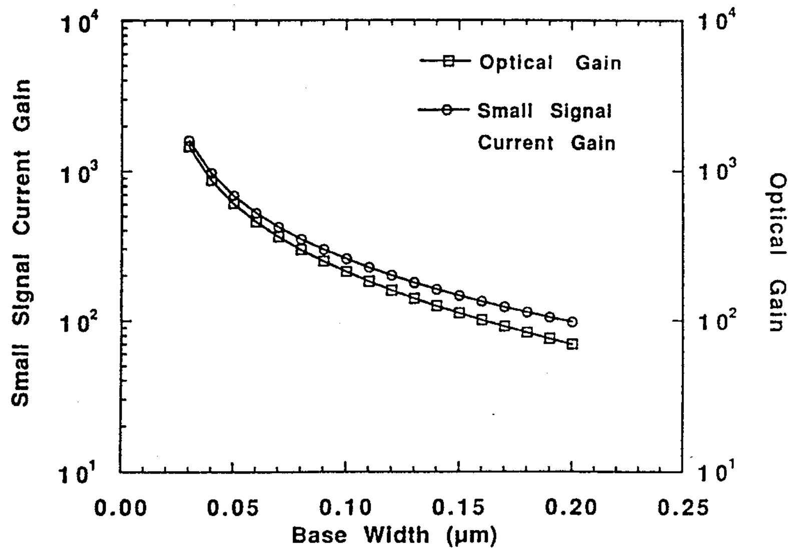

Figure 16 Optical gain and small signal current gain versus base width for the device structure of Chandrasekhar et al. [21] for a base doping of 7 x $10^{17}/cm^3$ for a constant optical power of 1 μW.

As seen in Figure 14 and discussed above, at low collector currents the model's calculated results over-estimate the optical gain. This discrepancy is expected at the lower collector currents because this model does not include in the small signal current gain calculation the effects of a number of the base recombination currents, such as the heterojunction interface and emitter-base space charge region components, which are known to dominate the base current at low emitter-base bias, have an ideality factor of two and which Ryum and Abdel-Motaleb [24] have shown reduce the small signal current gain at low collector current densities. Inclusion of these recombination currents would cause the small signal current gain, and so the optical gain, to show a stronger dependence on the collector current and a peaking effect at high current densities as is usually seen for the small signal current gain in HBTs.

As calculated in this model, the optical gain is independent of the incident optical power. This arises in part from the fact that the photocurrent components are each directly proportional to the optical flux density F_o. In addition, the model calculates the small signal current gain in the absence of light so the effects of the optically generated excess electron concentration in the base on the base recombination are neglected in the calculation of the small signal current gain. Experimentally, the optical gain was similarly observed to be nearly constant over a range of optical powers from approximately 0.7 to 10 μW, but decreasing at both lower and higher optical powers [21]. The fallfoff at high optical power could be due to increased recombination and an associated reduction in the current gain or due to base pushout effects. A more comprehensive model taking into account all of the base recombination currents as well as the effects of the optical power on the excess electron concentration in the base could help in understanding the falloff in optical gain at lower and higher optical power.

Since the wide energy bandgap emitter is nearly transparent at long wavelengths, initial optical absorption occurs in the quasi-neutral base for topside illumination where it generates the base component of photocurrent. Subsequent optical absorption occurs in the base-collector space charge region and the neutral collector where, in the latter case, only those carriers photogenerated within a diffusion length of the edge of the base-collector space charge region edge are collected. As a result, both the base and collector region widths and doping levels will have an impact on the photocurrent density and its components. Shown in Figure 15 is a plot versus the base width for a fixed base doping of $N_B = 7 \times 10^{17}/cm^3$ of the total photocurrent and each of the three components for a fixed optical power of 1 μW. As can be seen, the collector component g_cF_o and the base-collector space charge region J_{dpl} components are comparable in size and much larger than the base component. The component due to absorption in the base-

collector space charge region is large in size due to the relatively small attenuation by the thin base region of the light intensity it receives and the comparable size of the space charge region width (W_{BC} = 0.73 μm) and the optical absorption depth($1/\alpha_b \cong 0.66$ μm at 1.3 μm). The collector component is significant due to the fact that the collector width (W_C = 1.0 μm) is also comparable to the optical absorption depth but less than the hole diffusion length in the collector (L_{pc} = 2.9 μm) so that a substantial fraction of the photo-generated holes can be collected. But J_{dpl} is larger due to the fact that the light is incident from the top of the device so that the light intensity is greater entering the base-collector space charge region than the neutral collector below it. For the case of backside illumination used by Chandrasekhar et al. [21], the collector component dominates over the J_{dpl} and the total photocurrent is larger. As expected, both of these components are nearly independent of the base width, but do decrease as the base width increases due to a reduction in the light intensity received by each due to added base absorption (for frontside illumination). As a result, in Figure 15 the total photocurrent decreases by about 20% as the base width increases from 0.05 μm to 0.20 μm.

The third photocurrent component seen in Figure 15 is due to optical absorption in the quasi-neutral base and is much smaller (more than two orders of magnitude) than the previously considered components. Since the base width typically used for HPTs is about 0.2 μm, and that used for high performance, high frequency HBTs is even smaller (W_B < 0.1 μm), and both are much less than the optical absorption depth, the extent of optical absorption in the base region is nearly negligible as seen in Figure 15, but does increase with increasing base width as expected. As a result, increasing the base width to increase the base component of the photocurrent is not effective in increasing the total photocurrent so that a small base width for obtaining a high current gain is more advisable to achieve a high optical gain G.

For the HBT, the small signal current gain β is also known to be a strong function of the base width, decreasing rapidly with increasing base width as shown in Figure 16. For the light base doping of 7 x $10^{17}/cm^3$ used in the HPT of Chandrasekhar et al. [21] and others [9,10], the current gain decreases from more than a thousand at very small base widths to approximately 100 at W_B = 0.20 μm. By comparison, Chandrasekhar et al. [21] reported small signal current gains ranging from 90 to 800 for their devices, so our underestimation of the optical gain in Figure 14 can likely be attributed to our lower projections of the current gain. Since the HPT's optical gain is a product of the small signal current gain and the photocurrent, the results in Figures 15 and 16 can be combined to give the optical gain's variation with the base width W_B, which is also shown in Figure 16. As the base width increases, the sharp falloff in the current gain β and the slow decrease in the total photocurrent combine so that the optical gain G

decreases rapidly to less than 100 at W_B = 0.20 μm. Included in Figure 16 are the effects on the current and optical gains of the thermionic field emission at the emitter-base heterojunction and the finite electron concentration at the collector end of the base due to the non-negligible collector current density. Incorporation of the thermionic field emission acts to reduce the projected current and optical gains since it produces a reduced density of injected electrons at the emitter end of the quasi-neutral base. This gives rise to a reduced emitter and collector electron current components. Similarly, the finite electron concentration at the collector end of the base due to the non-negligible collector current reduces the electron gradient across the base reducing the base transport factor and, therefore, the current and optical gains.

The base doping can also be expected to impact the HPT's optical gain. It is known to influence the small signal current gain by reducing the electron minority carrier lifetime and diffusion length in the base as the base doping is raised [18]. In addition, the base-collector space charge region width also shrinks somewhat as the base doping is raised, the extent depending on the collector doping. For a fixed base width (W_B = 0.2 μm), the current gain decreases rapidly with increasing base doping as shown in Figure 17. At the same time, the

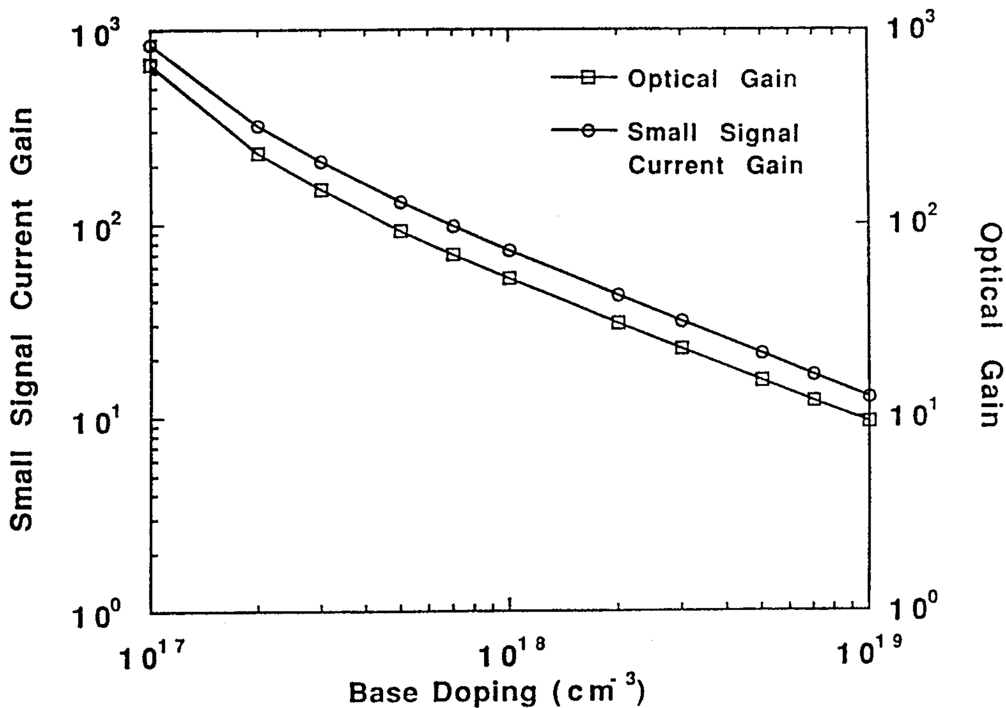

Figure 17 Optical gain and small signal current gain versus base doping for the device structure of Chandrasekhar et al. [21] for a base width of 0.20 μm for a constant optical power of 1 μW.

total photocurrent changes only slightly with increased base doping so that the optical gain falloff follows that of the current gain. As a result, the base width and doping should be set to optimize the transistor operation of the HPT, i.e. current gain and cutoff frequency, rather than selected to optimize the base's photocurrent component. Because one of the dominate components in the photocurrent as shown in Figure 15 is due to optical absorption in the collector, the effects of the collector width and doping on the photocurrent and optical gain are also important. Explored in Figure 18 for a fixed collector doping of 5 X $10^{15}/cm^3$ is the effect of the collector width. For collector layer thicknesses less than approximately 0.7 μm, the collector is completely depleted at small base-collector biases (< 1 V) and the contribution to the photocurrent from the neutral collector region disappears while that due to the base-collector space charge region becomes a constant due to the presence of the underlying highly doped subcollector. For thicker collectors than about 0.7 μm, the collector component of the photocurrent density increases almost linearly with increasing collector thickness, as expected, as the collector width is less the hole diffusion length in the collector (2.9 μm), but comparable to the optical absorption depth (0.66 μm). But the effect on the total photocurrent density is

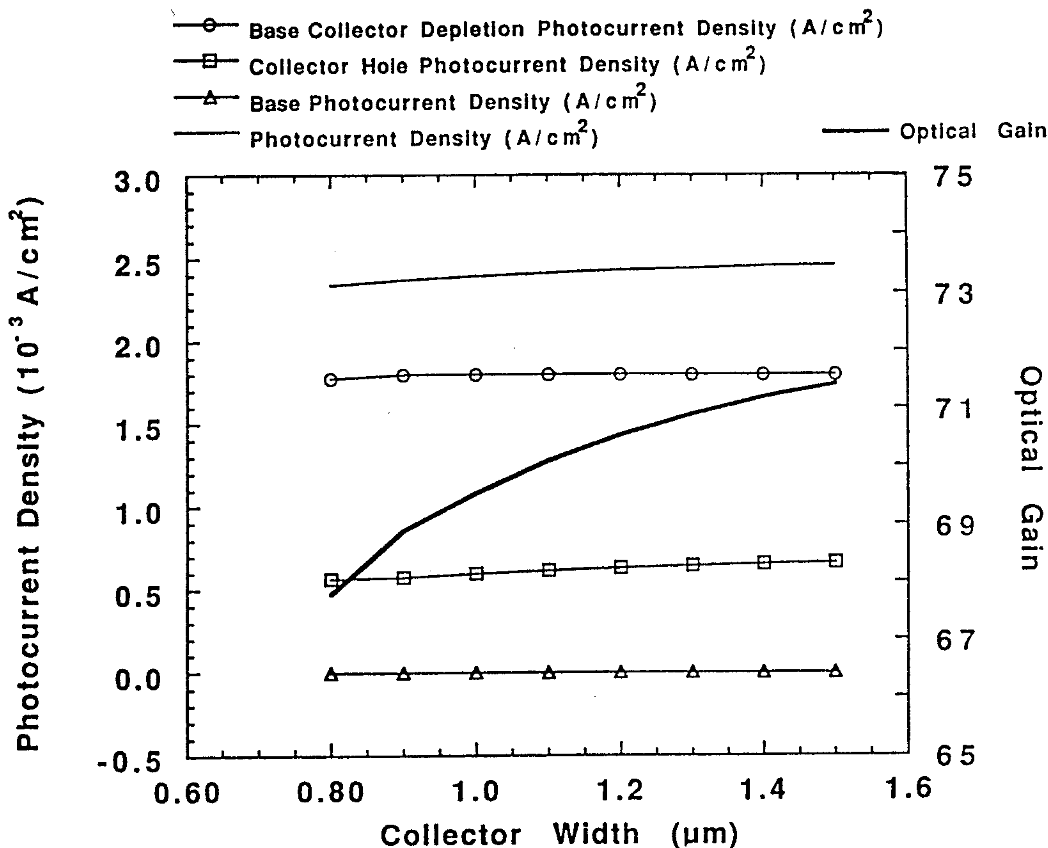

Figure 18 Total photocurrent density and components and optical gain versus collector width W_C for the device structure of Chandrasekhar et al. [21] for a collector doping of 5 x $10^{15}/cm^3$ for a constant optical power of 1 μW.

small since the photocurrent is dominated by the base-collector depletion region absorption for the case of frontside illumination. Since the small signal current gain is independent of the collector region width, the optical gain increases only slightly in conjunction with an increase in the collector region width as shown in Figure 18.

Finally, the collector doping has a finite effect on the HPT's performance, particularly above 1 X $10^{17}/cm^3$ as seen in Figure 19. As the collector doping increases, the base-collector space charge region width W_{BC} and the corresponding photocurrent component J_{dpl} decreases. However, for frontside illumination, the shrinking W_{BC} allows more light to enter the neutral collector and the collector component of the photocurrent increases. At the same time, as the collector doping increases, the minority carrier hole lifetime and diffusion length in the collector decrease so that the efficiency of collection of the photogenerated holes degrades.

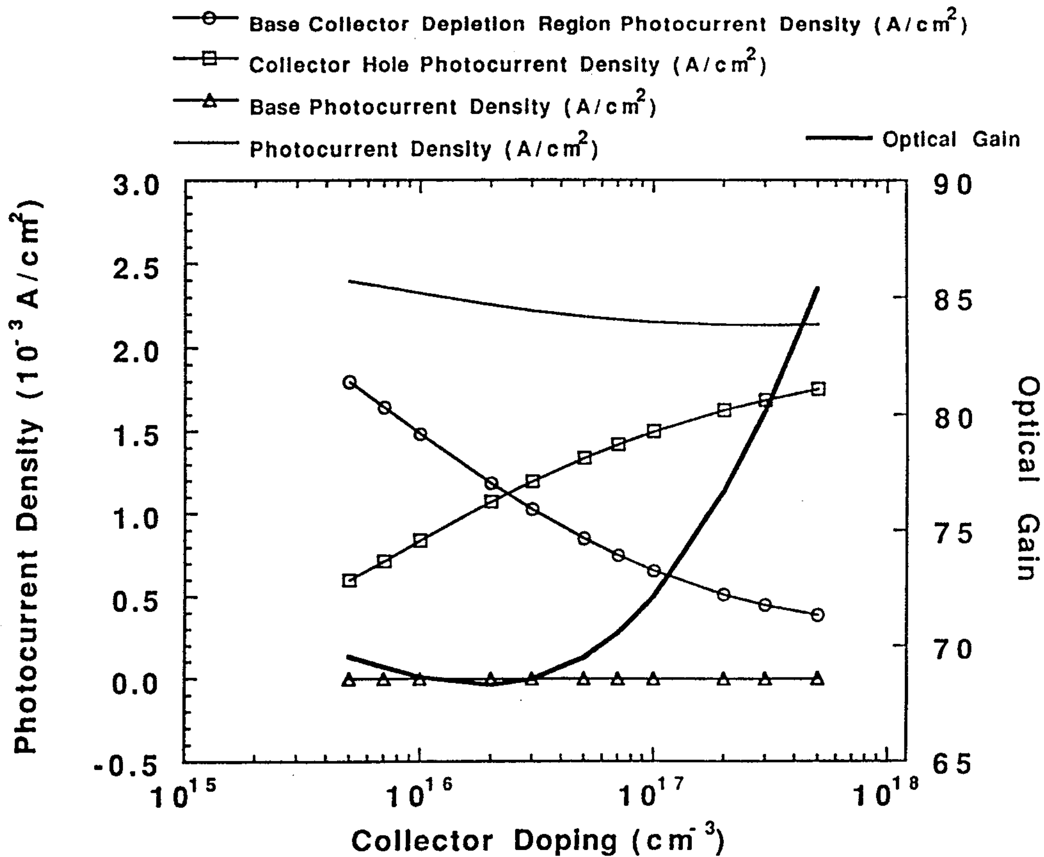

Figure 19 Total photocurrent density and components and optical gain versus collector doping for the device structure of Chandrasekhar et al. [21] for a constant collector width of W_C = 1.0 μm for a constant optical power of 1 μW.

Nevertheless, since the hole diffusion length is larger than the collector thickness (1.0 μm), the net effect is for the collector component to increase as seen in Figure 19. The combined effect on the total photocurrent of these two influences is to reduce the collector component slightly as the collector doping is increased. However, as the collector doping increases, the current gain increases so that the optical gain increases by approximately 20 % at 5 X $10^{17}/cm^3$ over that at low collector doping levels.

Further development of the model has been pursued to include the effects of the recombination currents on the base current to obtain a more realistic description of the device's current gain, particularly its dependence on the collector current density, and its optical gain. Ryum and Abdel-Motaleb [24] have described these recombination currents for the HBT in detail. In addition, the effects of optical absorption on the recombination currents should be included. The latter may help in understanding the falloff in the optical gain seen by Chandrasekhar et al. [21] at the higher optical powers. In particular, the development of an advanced Gummel-Poon model for the HPT operating in its three terminal configuration, but also including the effects of the optical absorption in the various regions of the device has been investigated [15,17]. The development of such a model follows from the previous work we have done in developing the thermionic-field-diffusion model described above, and from our previous HBT modeling work [18]. The primary advantage such a model would provide is that it would provide a useful tool in the determination of the appropriate DC bias point for optimum operation of the HPT and for guidance in the design of the epitaxial layer parameters for the device. Such a capability is extremely important for design high frequency optical receivers employing the HPT.

As an extension of the above described thermionic field emission model, a Gummel-Poon model for abrupt, single heterojunction Npn bipolar phototransistors has been developed including the effects of the dc base bias on the current and optical gains. The model has recently been reported [15,17]. In brief, initially, the excess electron concentration at the emitter end of the quasi-neutral base is determined by matching the thermionic field emission across the emitter-base heterojunction with the diffusion current at the emitter end of the base while including the effects of optical generation. The result is used in determining the electron profile in the base from which the base charge and the electron component to the emitter and collector currents are calculated following the Gummel-Poon model. The photocurrent's components due to optical absorption in the quasi-neutral base, the base-collector space charge region and the collector region are determined taking into account the nonuniform optical generation assuming topside illumination. A comprehensive description of the recombination current components is

incorporated including the effects of optical absorption on recombination. The model is then used to calculate the dc and small signal current gain and the device's optical gain, and to examine the effects of dc biasing and optical power level. The simulation results have been compared with the available experimental results and reasonable agreement found.

As an example, the model was applied to the simulation of the InP/InGaAs HPT recently reported by Chandrasekhar et al. [21] where the device structure and material parameters employed in the calculation are the same as those given previously in Table I, which are similar to those used elsewhere [9,10]. While this modified Gummel Poon model was developed assuming frontside illumination through the wide bandgap emitter (with the emitter metal and n+ contact layer removed except for contact stripes at the emitter mesa edges), Chandrasekhar et al. [21] employed an n+ indium phosphide subcollector and backside illumination. As a result, a rigorous comparison to their experimental results is not possible. In particular, the use of backside illumination results in greater absorption in the collector and less in the base region than for frontside illumination so that the effects of optical absorption on the base profile are less significant. This difference for frontside versus backside illumination becomes more significant at low DC base bias and high optical power. However, for more typical device operation, the total photocurrent density is nearly the same in magnitude for both front and backside illumination and the transistor's operation is not disturbed appreciably so that comparison of the calculated and measured optical gains is reasonable in the absence of other experimental data.

As a starting point, shown in Figure 20 is a Gummel plot of the total base and collector current densities in the absence of light (F_o=0) calculated for the HPT versus the emitter-base bias. Following [21], the device's geometry was taken to be 12 μm X 12 μm for the emitter-base junction and 20 μm X 33 μm for the base collector junction. Also included in the plot are the recombination current components important in accurately modeling the base current. As can be seen, for operation in the dark, nonradiative recombination in the quasi-neutral base dominates the base current except at very low bias as expected for an InP-based transistor. From these results, the DC current gain h_{FE} as a function of the collector current is calculated and plotted in Figure 21. Also shown in Figure 21 is the small signal current gain for the device. The results are typical of that expected for a InP-based heterojunction bipolar transistor (HBT) where the calculated current gain (250) is frequently found to be nearly a constant as a function of collector current density. By comparison, Chandrasekhar et al. [21] reported the experimental current gain at two biases, a current gain of 80 at a collector current of 1 μA and 600 at 10 mA. Comparison with these results suggests that our model

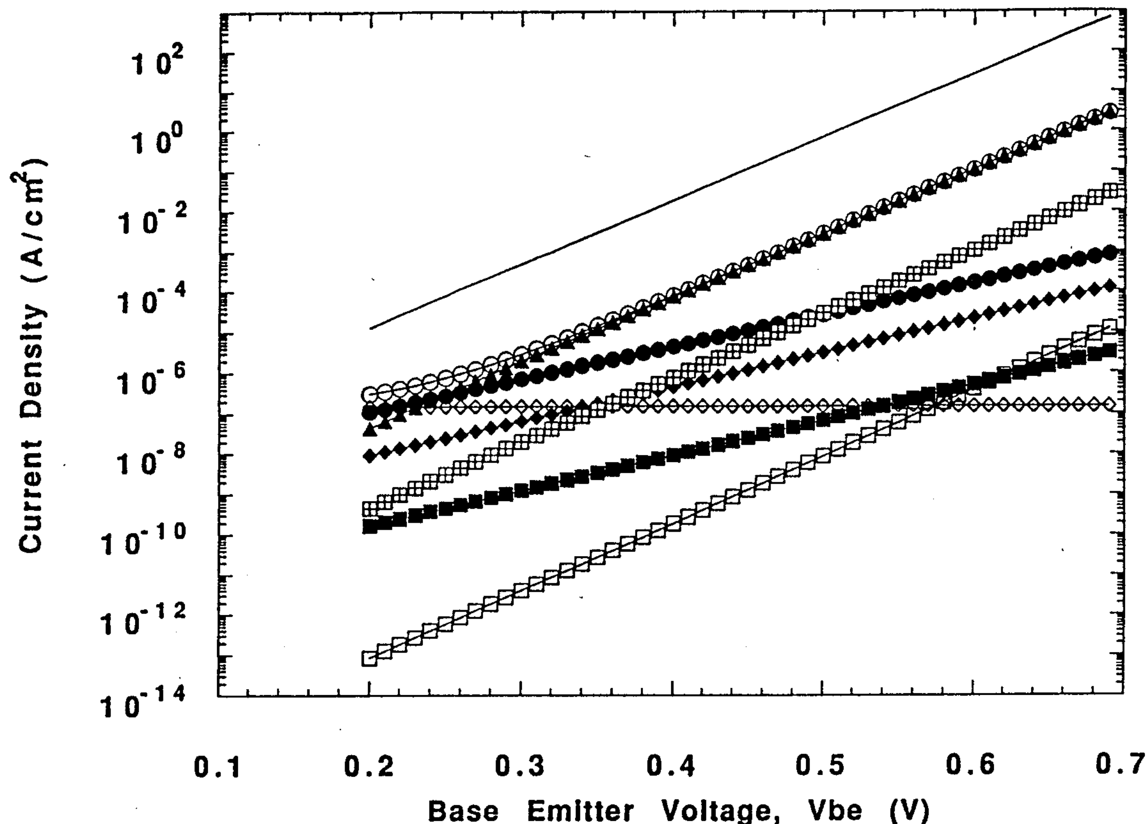

Figure 20 Gummel plot of total collector J_C (no symbol) and base J_B (○) current density and base recombination current components (nonradiative J_{br} (▲), radiative J_{rr} (□), surface J_{sr} (●), interface J_{ir} (◆), space charge region J_{scr} (■), hole back injection J_{ep} (□), and collector hole J_{cp} (◊)) versus emitter-base bias for the device of Chandrasekhar et al. [21] for no optical illumination (F_o=0).

somewhat underestimates the $2k_BT$ recombination currents at low bias, perhaps due to underestimating the surface, interface and space charge region recombination current components. At the higher biases, since the experimental current gain (600) is larger than our calculated value (250), the results also suggest that the base lifetime is somewhat underestimated in our model so that the base nonradiative recombination current and total base current are overestimated reducing the calculated gain. Since the base lifetime is known to be a function of the epitaxial quality, its value can vary significantly from one sample to the next. As a result, more exact agreement of our simulation results with the experimental current gain may not be reasonable.

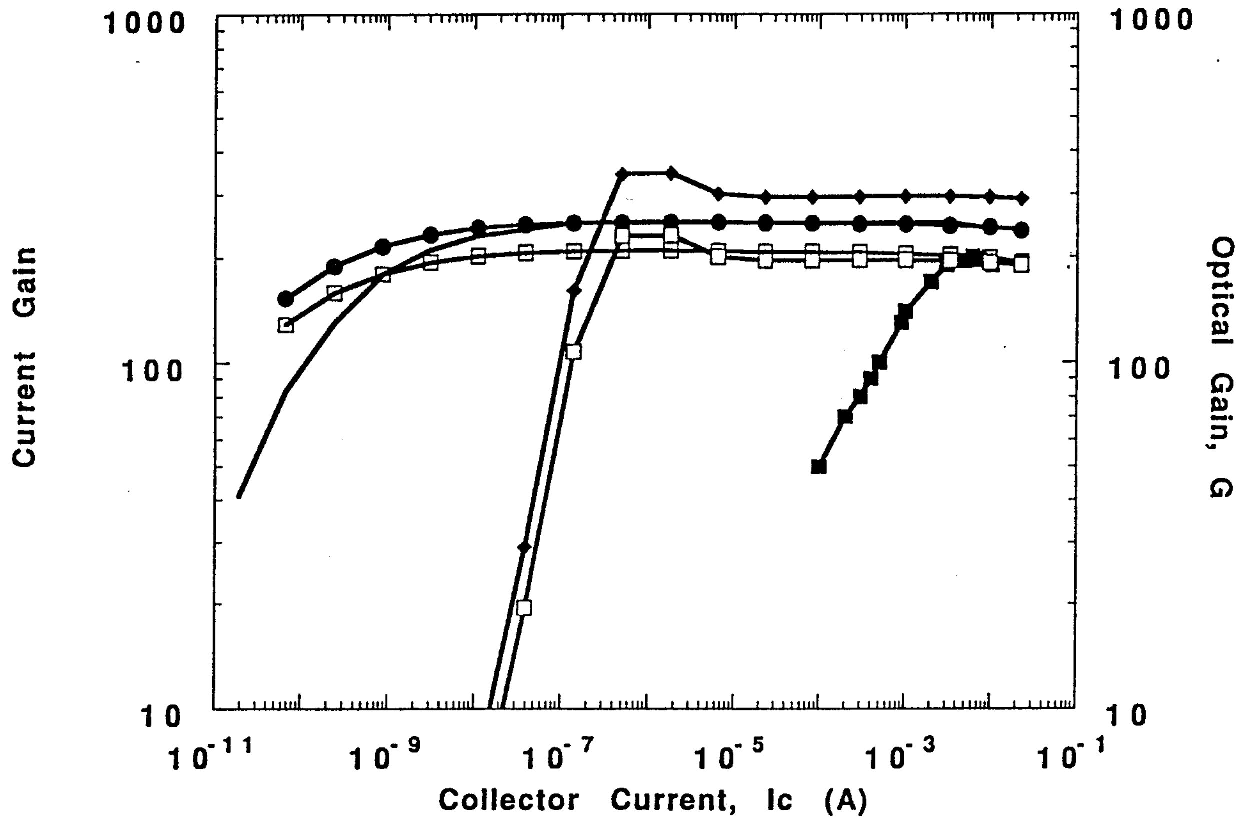

Figure 21 Calculated DC current gain in the dark (no symbol) and with light (◆) and small signal current gain (●) versus dc collector current for the device of Chandrasekhar et al. [21]. Also shown are the optical gain calculated using the dark current gain (□) and including optical effects on the current gain (□) compared with the experimental results (■).

Also shown in Figure 20 is the optical gain for the HPT calculated from the model as a function of the DC collector current in comparison with the experimental results from Chandrasekhar et al. [21] for an optical power of 1 μW. The experimental optical gain increases rapidly with increasing collector current with the gain peaking at 5 mA. This peaking corresponds primarily to the rise in the device's current gain with increasing collector current discussed above. At the peak, the measured and calculated optical gains are in good agreement. As seen in Figure 21, the calculated optical gain falls off at lower collector currents similar to the experimentally observed rolloff, though the onset of the falloff is at a much lower collector current than in the experimental case. This falloff in the calculated optical gain is due to the effects of the optical absorption on the recombination currents and current gain. As described previously, the excess carriers generated by optical absorption also give rise to increased rates

of recombination for the recombination currents [17]. At low base-emitter biases, these optical contributions to the recombination rates can be significant so that the base current is appreciably enlarged and the current and optical gains degraded. While the model correctly predicts this falloff at low bias levels, in this comparison with the results of Chandrasekhar et al. [21] it underestimates the magnitude of the effect. This is probably due to the fact that the model underestimates, as described above, the magnitude of the $2k_BT$ recombination currents at low biases and so overestimates the current gain at low collector currents. Finally, at the highest collector currents, a rolloff in the current gain is expected due to base pushout which leads to degradation in the optical gain. In addition, the Gummel-Poon model employed here predicts an increase in the base charge q_b at high collector current densities so that the photocurrent component J_{op} will also decrease. Together, these effects are expected to produce a falloff in the optical gain at high collector current densities (10^4 to 10^5 A/cm^2), which is only partly shown in Figure 21 but experimentally observed by Chandrasekhar et al. [21].

The effects of optical illumination on HPT performance can be better understood by examining the effects of the photocurrent components on the device's terminal currents. Seen in Figure 22 is a Gummel plot for the device of Chandrasekhar et al. [21] of the total base and collector currents including the effects of optical illumination at 1 μW. Also included are the dominant photocurrent and base recombination current components. The results show several interesting features of HPT operation. First, at low emitter-base bias the photocurrent components dominate the base recombination currents and, in fact, give rise to a reversal in the base current since they produce hole injection into the base. This can also be understood from the base terminal current expression where the photocurrent terms have the opposite sign from the recombination currents. Second, at very low emitter-base bias, the extent of electron injection from the emitter is small and the collector current is dominated by the photocurrent so that the transistor action is unimportant and the device's operation reduces to that of a p-i-n photodiode. As a result, the collector current becomes a constant independent of the emitter-base bias as seen in Figure 22. Note, however, that the collector current does not reverse sign like the base current at low bias since the photocurrent contribution is positive. Third, as a result of optical absorption, there are also significant increases in some of the recombination current components, by as much as 10^4 in the case of the emitter-base space charge recombination J_{scro}. In the case of the nonradiative base recombination component J_{bro}, at low bias the component is independent of the bias because photoabsorption is providing the carriers for recombination instead of electron injection from the emitter.

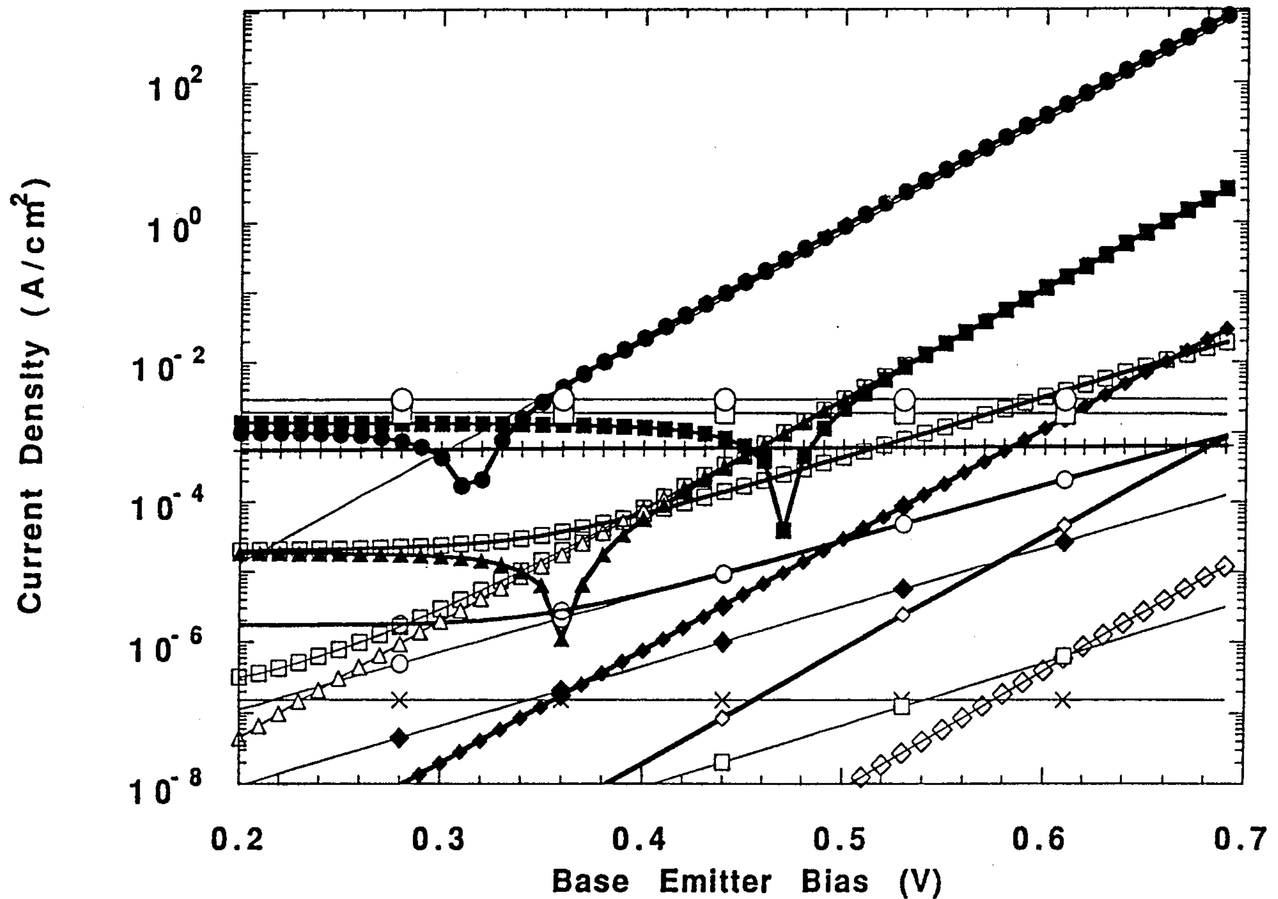

Figure 22 Gummel plot of total collector current density with J_{co} (●) and without light J_c (no symbol) and total base current density with J_{bo} (■) and without light J_b (□) versus emitter-base bias for the device of Chandrasekhar et al. [21] for optical illumination at 1 μW. Also included are the total photocurrent density J_{ph} (O) and dominant space charge region component J_{dpl} (□). Also shown are the base recombination current components with and without the light, respectively, (nonradiative J_{bro} (▲) and J_{br} (Δ), radiative J_{rro} (♦) and J_{rr} (◆), surface J_{sro}(O) and J_{sr} (O), space charge region J_{scro} (□) and J_{scr} (□), hole back injection J_{epo} (◊) and J_{ep} (◊), and collector hole J_{cpo} (+) and J_{cpo} (x), and interface J_{ir} (◆)).

For the HPT, the illumination of the device generates photocurrent components that contribute to the base current corresponding to optical absorption in the quasi-neutral base, the base-collector space charge region and in the neutral collector. Seen in Figure 23 is a plot of these components and the total photocurrent density versus the optical power calculated for the same device described above. As can be seen, the dominate component is that due to absorption in the base-collector space charge region. The smallest component arises from

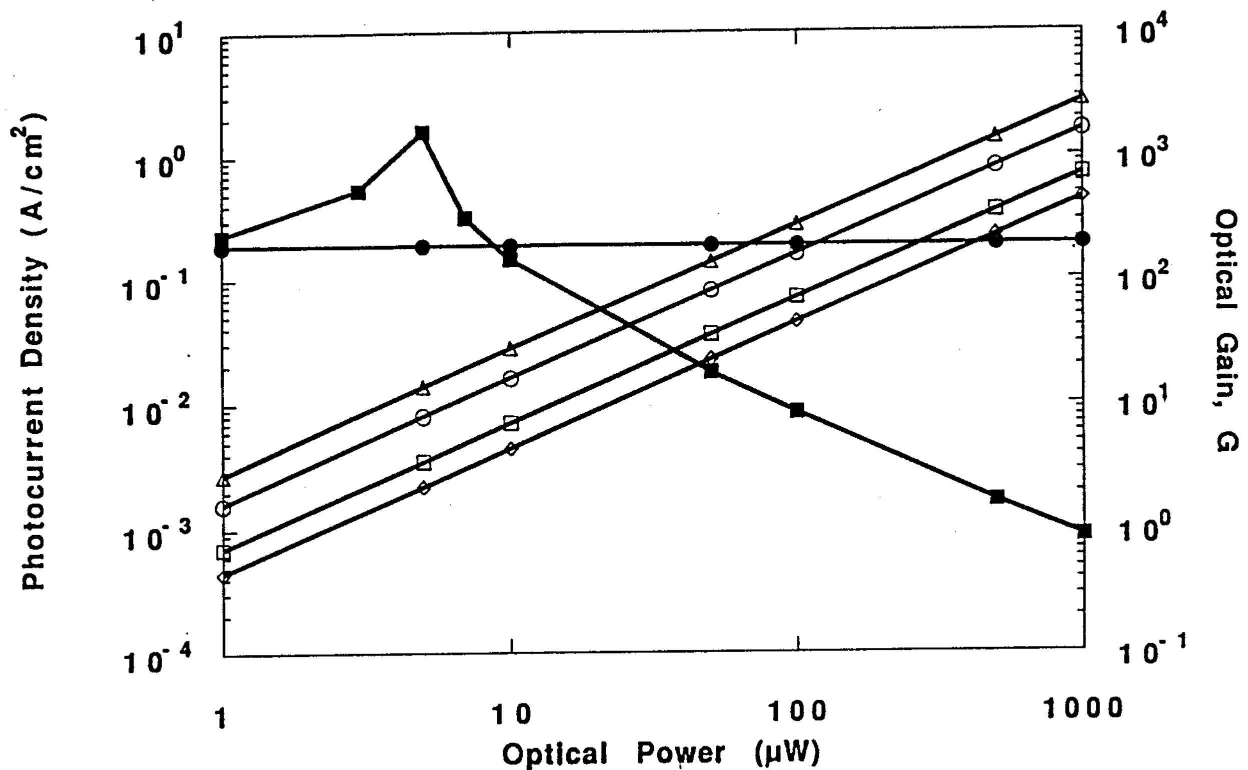

Figure 23 Calculated total photocurrent (Δ) and component densities (space chare region J_{dpl} (O), base J_{op} (◊) and collector $(J_{pc})_{opt}$ (□)) as a function of optical flux density F_o for the device of Chandrasekhar et al [21]. Also shown is the optical gain at low (■) and high (●) DC collector current density.

absorption in the quasi-neutral base, even for the case of frontside illumination assumed in this model, since the base width (0.2 μm) is much less than the optical absorption length ($1/\alpha_b$ =0.66 μm). It is also interesting to note from Figure 23 that the photocurrent densities can be substantial, i.e. > 10^{-3} A/cm^2 at optical power levels > 1 μW. By comparison with the current densities seen in Figure 22 for the base current, the photocurrent density at the higher optical powers can be seen to be comparable or larger than the base current density even when the HPT is biased at a significant DC base bias. As a result, the device's transistor operation can be modified when the optical power becomes large enough. To investigate this further, the device's optical gain was calculated as a function of the optical power for two different DC base biases giving rise to collector current densities of 1.2 A/cm^2 and 1.5 x10^4 A/cm^2 and the results included in Figure 23. As can be seen, at the higher DC bias, which is typical of that employed for an HBT, the optical gain is a constant independent of the optical power. However, at the lower bias level, the effects of optical absorption at higher optical powers modify the

transistor's operation and degrade the optical gain. The peaking seen in the optical gain seen in Figure 23 arises from the reversal in the base current that occurs as the optical power rises. This corresponds to the reversal in the base current discussed above and seen in Figure 22 for a constant optical power as the base-emitter bias increases. In summary, as a result of added recombination, the dc current gain for the device is reduced by the effects of optical absorption at low base-emitter bias as seen in Figure 22. This, in turn, produces a reduction in the device's optical gain at low collector currents also seen in Figure 22. Alternatively, for a fixed dc base bias, as the incident optical power rises, the effects of optical absorption eventually produce a degradation in the optical gain as seen in Figure 23.

Finally, for HPT operation in optical receivers, the use of the dc base bias produces a dc collector current that adds shot noise that may impact the device's signal-to-noise ratio. Further study is needed to determine an optimum dc bias so as to optimize the device's current and optical gains, but without introducing excessive noise into the receiver's operation. To do the analysis and design, it would also be useful to model the HPT's various noise components and the effects on them of device biasing and epitaxial structure. Preliminary work has been undertaken here in this direction with a development of a noise modeling capability for the HBT[25].

As a final element in the work and the final objective, the above described HPT experimental and theoretical development have been used to develop integrated optical receivers for high frequency applications, such as the phased array application described by Daryoush [1]. A mask set that has been developed and fabricated for use in developing HPT-HBT based optical receivers. Included in the mask layout are several designs for receivers including ones with the HPT configured in the two and three terminal configurations. Also included are the HPT connected in various amplifier configurations including the simple, single stage common emitter amplifier and multi-stage amplifiers. Finally, several feedback amplifiers have also been included in the mask layout including ones with an HBT used as a variable feedback resistor. Further work is continuing in fabrication and characterization of these optical receivers using the new Hughes HBT wafer, and receiver and mask redesign, if needed, to develop the desired receiver characteristics. Preliminary fabrication runs with the above described mask set have been made. While the low gain of the HBT's and HPT's in the initial run were due to the poor epitaxial layer quality, the successful fabrication of the receivers as seen in the figure demonstrates the feasibility of the fabrication process. With the better epitaxial material received from Hughes, working receivers with the desired microwave capabilities are feasible and will be demonstrated.

References

1. A. S. Daryoush, "Optical Synchronization of Millimeter-Wave Oscillator for Distributed Architecture," IEEE Trans. Microwave Theory Tech., vol. 38, pp. 467-476 (1990).
2. P. R. Herczfield, A. S. Daryoush, A. Rosen, A. K. Sharma and V. M. Contarino, "Indirect Subharmonic Optical Injection Locking of a Millimeter Wave IMPATT Oscillator," IEEE Trans. Microwave Theory Tech., vol. 34, pp 1371-1376 (1986).
3. S. Chandrasekhar, B. Glance, A. G. Dentai, C. H. Joyner, G. J. Qua and J. W. Sulhoff, "Monolithic Balanced p-i-n/HBT Photoreceiver for Coherent Optical Heterodyne Communications," IEEE Photon. Tech. Lett., vol. 3, p 537 (1991).
4. M. Govindarajan and S. R. Forrestt, "Design Considerations for Wide-Band p-i-n/HBT Monolithic Transimpedance Optical Receivers," J. Lightwave Technol., vol. 11, p 367 (1993).
5. T. Horimatsu, T. Iwama, Y. Oikawa, T. Touge, M. Makiuchi, O. Wada and T. Nakagami, "Compact Transmitter and Receiver Modules with Optoelectronic-Integrated Circuits for Optical LAN's," J. Lightwave Tech., vol. 4, p 680 (1986).
6. B. Jalali and R. N. Nottenburg, "Heterostructure Bipolar Transistors" Ch 12 in **Indium Phosphide and Related Materials: Processing, Technology and Devices**, A. Katz, Ed., Artech House, Boston p 379 (1992).
7. Y. K. Chen, R. N. Nottenburg, M. B. Panish, R. A. Hamm and D. A. Humphrey, "Subpicosecond InP/InGaAs Heterojunction Bipolar Transistors," IEEE Electron Dev. Lett., vol. 10, p 267 (1989).
8. Y. Matsuoka and E. Sano, "InP/InGaAs Double-Heterojunction Bipolar Transistors for High-Speed ICs and OEIcs," Solid State Electr., vol. 38, p. 1703 (1995).
9. J. C. Campbell, "Phototransistors for Lightwave Communications," Ch 5 in Semicond. and Semimetals, vol. 22, part D, p 389, W. T. Tsang, Ed. Academic Press, Orlando (1985).
10. D. C. Scott and H. R. Fetterman, "Millimeter Wave Generation Using InP HBT Phototransistors," Ch 10 in *InP HBTs: Growth, Procesing and Applications*, B. Jalali and S. J. Pearton, Ed., Artech House (1995).
11. E. Suemaatsu and H. Ogawa, "Frequency Response of HBTs as Photodetectors," IEEE Microwave & Guided Wave Lett., vol. 3, p 217 (1993).
12. T. F. Carruthers, M. Y. Frankel and C. S. Kyono, "Ultrafast Photodetection with an AlInAs/InGaAs Heterojunction Bipolar Transistor," Appl. Phys. Lett., vol. 63, p 1921 (1993).

13. H. Kamitsuna, "Ultra-Wideband Monolitic Photoreceivers using Novel HBT-Compatible HPT's with Novel Base Circuits, and Simultaneously Integrated with an HBT Amplifier," J. Lightwave Technol., vol. 13, p 2301 (1995).
14. S. M. Frimel and K. P. Roenker, "A Thermionic-Field-Diffusion Model for Npn Bipolar Heterojunction Phototransistors," accepted for publication in J. Appl. Phys.
15. S. M. Frimel and K. P. Roenker, "A Gummel-Poon Model for Npn Bipolar Heterojunction Phototransistors," accepted for publication in J. Appl. Phys.
16. S. M. Frimel and K. P. Roenker, "Design of an Integrated Optical Receiver for a Phased Array Antenna," Proc. 39th IEEE Midwest Symp. Circuits and Systems, p 1363 (1996).
17. S. M. Frimel and K. P. Roenker, "Use of DC Base Bias for Enhancing the Performance of Heterojunction Bipolar Phototransistors," to be published in Proc. of XXVI State of the Art Program on Compound Semiconductors, vol. 97-1, (1997).
18. T. Conklin, S. Naugle, S. Shi, S. Frimel, K. P. Roenker, T. Kumar, M. M. Cahay and W. E. Stanchina, "Inclusion of Tunneling and Ballistic Transport Effects in an Analytical Approach to Modeling on NPN InP-based Heterojunction Bipolar Transistors," J. Superlattices and Microstructures, vol. 18, pp. 21-32 (1995).
19. M. Hafizi, W. E. Stanchina, R. A. Metzger, P. A. MacDonald and F. Williams, "Temperature Dependence of DC and RF Characteristics of AlInAs/GaInAs HBT's," IEEE Trans. Electron Dev., vol. 40, p. 1583 (1993).
20. M. Hafizi, W. E. Stanchina, R. A. Metzger, J. F. Jensen and F. Williams, "Reliability of AlInAs/GaInAs Heterojunction Bipolar Transistor's," IEEE Trans. Electron Dev., vol. 40, p. 2178 (1993).
21. S. Chandrasekhar, M. K. Hoppe, A. G. Dentai, C. H. Joyner and G. J. Qua, "Demonstration of Enhanced Performance of an InP/InGaAs Heterojunction Phototransistor with a Base Terminal," IEEE Trans. Electron Dev. Lett., vol. 12, pp. 550-2 (1991).
22. A. A. Grinberg, M. S. Shur, R. J. Fischer and H. Morkoc, "An Investigation of the Effect of Graded Layers and Tunneling on the Performance of AlGaAs/GaAs Heterojunction Bipolar Transistors," IEEE Trans. Electron Devices, vol. 31, pp. 1758-65 (1984).
23. M. B. Das, in *HEMTs and HBTs: Devices, Fabrication and Circuits* , Edited by F. Ali and A. Gupta (Artech House, Boston, 1991) Chap. 4, p. 191.
24. B. R. Ryum and I. M. Abdel-Motaleb, "A Gummel-Poon Model for Abrupt and Graded Heterojunction Bipolar Transistors (HBTs)," Solid State Electron., vol. 33, pp. 869-80 (1990).
25. E. Suematsu and N. Imai, IEEE Trans. Microwave Theory Tech. **44**, p. 133 (1996).